TAMPEREEN TEKNILLINEN YLIOPISTO
TAMPERE UNIVERSITY OF TECHNOLOGY

ALI ZAIB RABBANI

MODELING OF GRID CONNECTED PV GENERATOR FOR POWER FLOW ASSESSMENT

Master of Science thesis

Examiner: Prof. Enrique Acha
Examiner and topic approved by the Faculty Council of Computing and Electrical Engineering
on October 5th, 2016

ABSTRACT

ALI ZAIB RABBANI: Modeling of Grid Connected PV Generator for Power Flow Assessment
Tampere University of technology
Master of Science Thesis, 61 pages, 6 Appendix pages
Master's Degree Programme Electrical Engineering
Major: Smart Grids
Examiner: Professor Enrique Acha

Keywords: PV, DC-DC Converter, DC-AC Converter, VSC, Power Flows, Distribution Generation, MATLAB

The power distribution systems are continuously expanding due to the rise in world population and its migration to urban areas. But consuming the non-renewable resources to generate the electric power, the carbon emissions have made a serious call to global warming so, during the last decade, the electric power systems have seen the penetration of renewable energy resources. This phenomenon has given flexibility to the power grid but also its complexity has increased. In order to successfully integrate the distribution generation of the renewable energy resources, the power grid demands modern power electronic equipment and state-of-the-art techniques, control approach and simulation tools to assess the practical like conditions of the systems.

In this continuous struggle to modernize and advance state-of-the-art power grid, this master research thesis investigates the two-stage converter topology for the grid-connected photovoltaic generator using the Newton Raphson iterative method in MATLAB programming. The reason to choose the photovoltaic generator is the rapid growth of such systems and the Newton Raphson method has the advantage of being fast in convergence and robust. The analytical tool for this research thesis is MATLAB coding.

The maximum power point tracking of the photovoltaic generator was applied in MATLAB coding to always extract the maximum power from the photovoltaic panels. Later on the admittance matrix, nodal voltages, linearized system of equations of the dc converter are constructed. Then this system of equations is incorporated into the linearized system of equations of the voltage source converter. To implement this scenario in power flows the dc converter implementation in power flows is also represented. The results of different test cases indicate that the two-stage converter topology, involving dc/dc and voltage source converter, for the distribution generation improves the voltage profile significantly at each bus of the system and inject the active power into the nodes generated by the DG units.

PREFACE

This Master of Science thesis was written at the Department of Electrical Energy Engineering at Tampere University of Technology under the supervision of Professor Enrique Acha.

At this point, I would like to thank my supervisor Prof. Enrique Acha for his continuous guidance and feedback throughout the research work. I learned a lot from his technical expertise, research and experience in the field of electric power engineering.

I would also like to thank my friends; Adnan, Aitzaz, Mukesh, Qutab, and Waqas for their continuous encouragement. I shall cherish the time we spent together here in Tampere, Finland.

Last, but not the least, I would like to dedicate this research thesis to my parents, Ghulam Rabbani and Zaib-un-Nisa, and my siblings, Hira Ahmad and Muhammad Abu Bakar for their endless support throughout my life.

Tampere, September 2017

Ali Zaib Rabbani

CONTENTS

LIST OF ABBREVIATIONS AND SYMBOLS

ABBREVIATIONS

AC	Alternating Current
BCM	Boundary Conduction Mode
Btu	British Thermal-Unit
CCM	Continuous Conduction Mode
CSC	Current Source Converter
CSP	Concentrated Solar Power
DC	Direct Current
DG	Distribution Generation
DCM	Dis-continuous Conduction Mode
FACTS	Flexible AC Transmission Systems
GTO	Gate Turn-Off Thyristor
IGBT	Insulated Gate Bipolar Transistor
IGCT	Insulated Gate Commutated Thyristor
I-V	Current-Voltage
LV	Low Voltage
MPP	Maximum Power Point
MV	Medium Voltage
NR	Newton-Raphson
OECD	Organization for Economic Cooperation and Development
p.u.	per unit
PV	Photovoltaic
PVG	Photovoltaic Generator
P-V	Power-Voltage
PWM	Pulse Width Modulation
SCR	Silicon Controlled Reactor
STATCOM	Static Compensator
VSC	Voltage Source Converter

SYMBOLS

A	Ideality factor of the diode
B	Electrical susceptance
D	Duty cycle
f_s	Switching frequency
G	Irradiance
G_o	Conductance
I_o	Diode saturation current
I_{sh}	Short-circuit current
Ln	Natural log
m_a	Amplitude modulation
P	Active power
Q	Reactive power
q	Electron charge
R	Resistance
R_s	Series resistance

R_{sh}	Shunt resistance
S	Complex power
T	Temperature
T_s	Switching time
t_{off}	Off-time
t_{on}	On-time
V_{oc}	Open-circuit voltage
W	Watt
X	Reactance
Y	Admittance
θ	Voltage angle
$\emptyset$	Phase shifter angle
Δ	Delta

1. INTRODUCTION

The population of the world and its migration to metropolitan areas is growing rapidly. In order to make human life more comfortable the advancement in technologies has become more needed than ever, especially the technologies driven by electricity. The utilization rate of electricity defines the economic prosperity of a country and the continuity of an electric power supply has been the essential stipulation for social development. Concerning to address this issue, the electric power networks have undergone fierce extension to meet the global demands which have highlighted the bigger challenges in electricity supply. According to International Energy Outlook 2016, global energy requirement has been surged and is expected to rise by 48% from the year 2012 to 2040 [1]. The History and future projection of energy consumption in Organization for Economic Cooperation and Development (OECD) and non-OCED regions, from the year 1990 to 2040 is graphically presented by quadrillion British Thermal Units (Btu) in Figure 1.1.

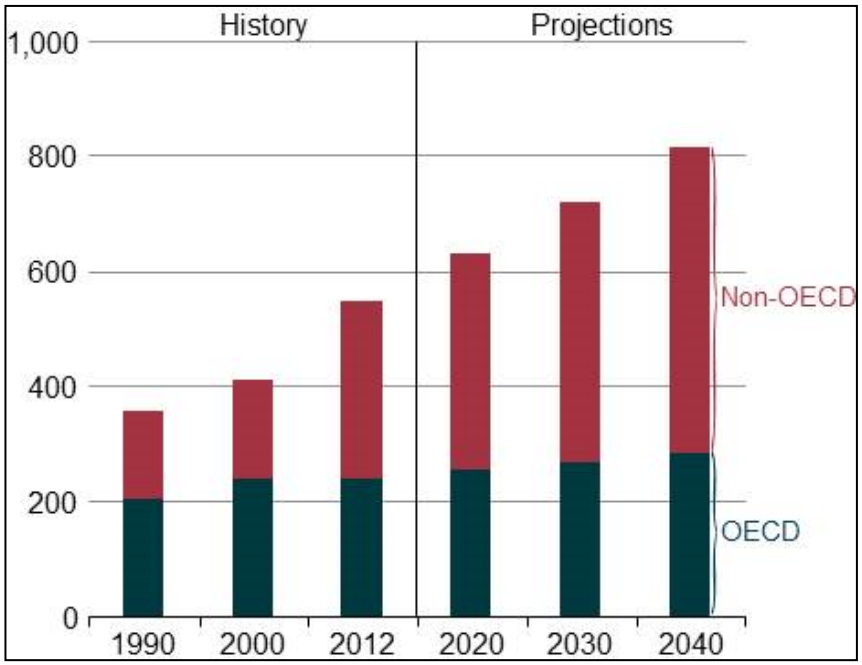

Figure 1.1. *World energy consumption* ***[1]***.

Electricity can be generated from various sources and transmitted by the means of power lines for industrial and domestic usage. These resources are mainly classified into two

catogories; renewable and non- renewable energy. The resources which are going to vanish and cannot be used repeatedly are called non-renewable resources which include coal, natural gas, nuclear energy and oil. Renewable resources; wind, solar, wave, hydroelectric, geo thermal and biomass, can be used regularly and not going to exhaust. These means of energy production are also useful in reducing the carbon emissions. Figure 1.2 gives an overview of energy resources.

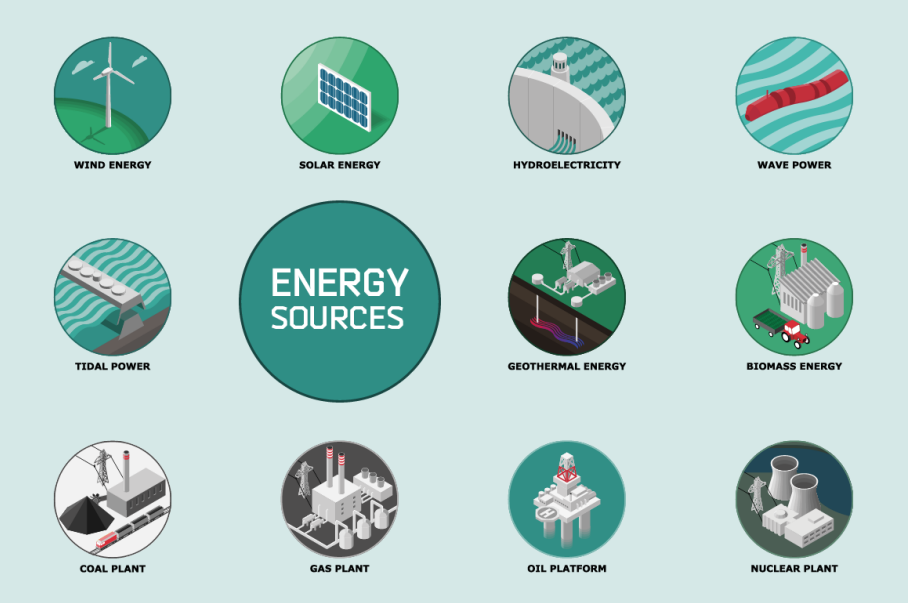

Figure 1.2. *Energy sources* ***[2]***.

By the year 2010, approximately 87% of total energy was achieved by non-renewable sources, whereas renewable sources had only 7% share [3]. Power generation from non-renewable sources has made a serious call to global warming and carbon emission. Due to the fact of limited fossil fuels and global emissions [3], the penetration of renewable energy sources to the electric power system has seen an increment in recent years and new investments have been made by many countries as represented in Figure 1.3.

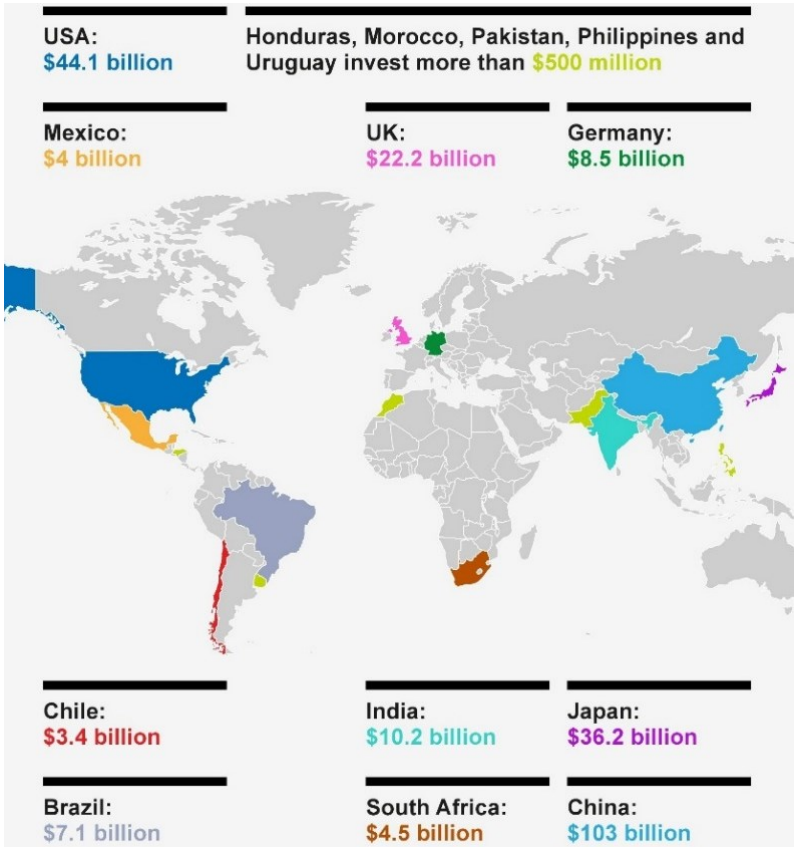

Figure 1.3. *New investment in renewable energy by country* ***[4]***.

In the past fifteen years, Photo-Voltaic (PV) systems have increased by 45% each year [5] and Concentrated Solar Power (CSP) is showing a growth rate of 35% annually [6].

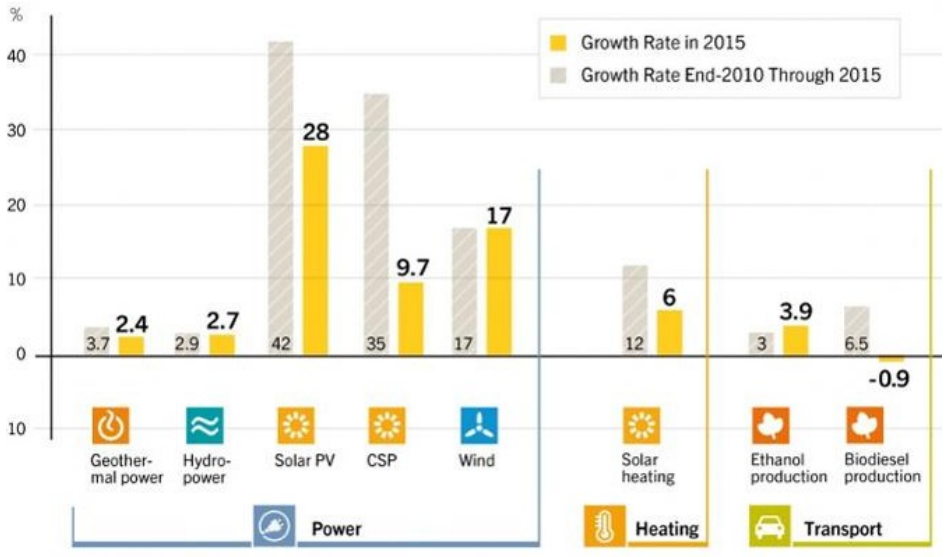

Figure 1.4. *Renewable 2016 global status report* ***[6]***.

In modern days the operational complexity of electric power networks has increased significantly, as most of the renewable energy sources require sophisticated power electronic equipment to incorporate into the AC grid. This whole Distributed Generation (DG) phenomenon comes at a time when large parts of the electric power grid have aged. The replacement of transmission lines, generators, transformers and protection equipment is an unavoidable fact which would give the opportunity to modernize electric power grid and significantly improving the continuity of the electricity supply to the end consumer. Besides the new equipment, modern control tehnologies and new practices should be adopted, laying the basis of the future smart grid.

1.1 Main concepts

The concepts, analytical tools and methods which will be addressed in this thesis are the following:

- PV generator (PVG)
- Voltage Source Converter (VSC)
- Buck-Boost converter
- Power flows

1.1.1 PV generator

Power electronics converters are used to feed energy to the utility grid, obtained from the series of solar panels called PV generator. This phenomenon is achieved by two main approaches: single stage and double stage topology. The former is comprised of only one DC to AC converter, whereas the latter includes one DC to DC and one DC to AC converter to enable maximum power from the solar panels [7] and it is used in this research.

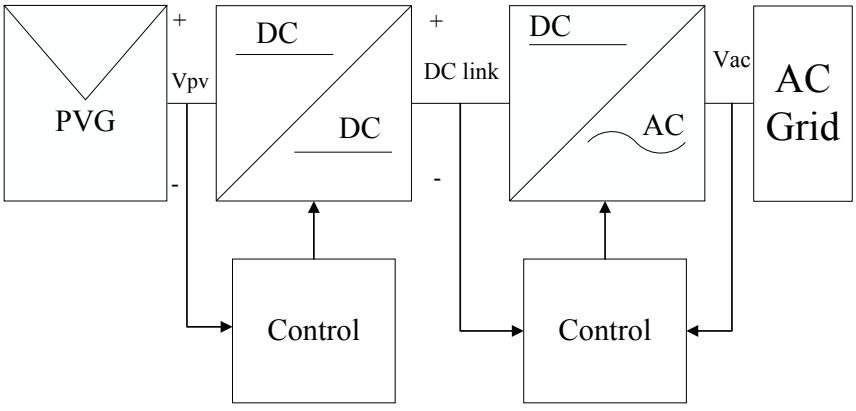

Figure 1.5. *Double stage grid connected PV generator* ***[7]****.*

1.1.2 Voltage source converter

In order to enhance the system stability and flexibility of the grid, the use of power electronic equipment has seen an increment, specifically by using VSC. The most recent innovations in power electronics are attracting manufacturers to undertake the new designs for VSC and launch them into the global market that will open the door for so many applications in near future. VSC converts DC to AC voltage and vice versa. An advance VSC model has been studied deeply to understand and control the power system parameters by using NR iterative method in power flows.

1.1.3 Buck-Boost converter

In recent years, switched mode power supplies have been used quite comprehensively in power electronic applications [8] and the buck-boost converter belongs to this block to build the grid connected power converters. The sole objective of the buck-boost converter is to step-up or step-down the voltage to the desired level via duty cycle/switching frequency.

1.1.4 Analytical tool

The major analytical tool used in this research thesis for power flow assessment is power flow algorithm, using Newton-Raphson (NR) method in MATLAB script. MATLAB programming has an edge over Simulink when it comes to assess and analyze the power flows of large electric networks as it consumes very less time in simulation and editing is quite easy by just adding some lines of coding. The NR method is used conveniently because of being robust and fast in nature for both small and large power systems.

1.2 Research objectives

The main objectives of this research presented in this thesis, given below:

- To model the series and parallel cells of solar panels in MATLAB code by carefully selecting the series and shunt resistances to obtain desired power under ideal operating conditions.
- To elaborate the admittance matrix and nodal power equations of VSC.
- To develop the admittance matrix and nodal power equations of the buck-boost converter under steady-state conditions and extend the admittance matrix carefully with VSC.
- To carry out the power flow simulations for the grid connected PV generator.

1.3 Thesis outline

This document is structured as follows. Chapter 1 provides the introduction about the energy consumption and role of renewable resources; especially solar panels, in power systems and future smart grids. Chapter 2 discusses the operation of photovoltaic power systems. Chapters 3 gives an overview of the power electronics, mainly focusing on VSC and DC-to-DC converters. Chapter 4 presents the power flows followed by mathematical modeling of VSC and buck-boost converter. Simulation results are presented in Chapter 5.

2. PHOTOVOLTAIC SYSTEMS

2.1 Introduction

This chapter provides an overview of the fundamental operating principle to utilize the energy of the Sun and converting into the electric power by the means of modern PV systems. The nuclear reactions occurring within the Sun result in a huge amount of solar energy, travelling through the space and ultimately reaching the atmosphere of the Earth in the form of rays. This solar energy is expressed as "irradiance *G",* having a constant value 1366 W/m^2 at the outer edge of Earth's atmosphere [9].

2.2 Photovoltaics

2.2.1 Construction and operation of solar cell

Electrical energy is extracted from a photovoltaic cell by utilizing the phenomenon called *photoelectric effect* [10], as PV cell is constructed by using two semiconductor materials, p-type and n-type.

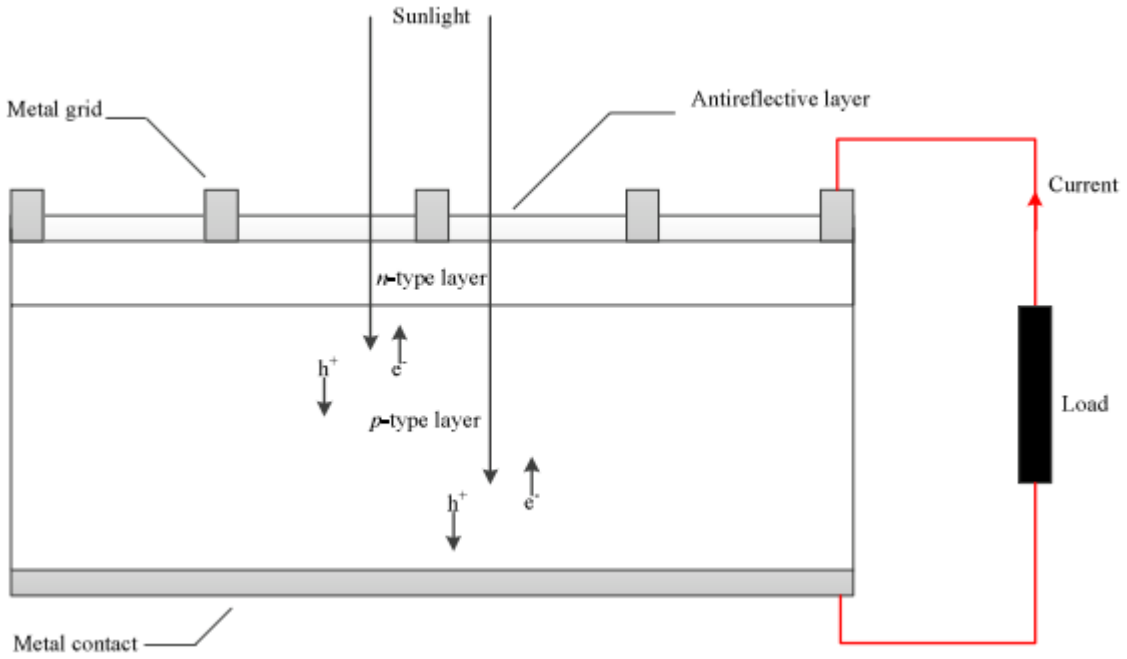

Figure 2.1. *Structure of a PV cell [adapted from 8].*

Figure 2.1 highlights the main parts and operating principle of a solar cell. As both semiconductor materials have different electric properties, positive and negative charges are

diffused in the opposite sides of the material interface that enables the operation of an electric field. As sunlight or solar radiation hit the solar cell then engaged with semiconductor material, electrons and holes [10] are released to conduction and the valence band. A preformed electric field makes electrons and holes move freely, they end up on the opposite side of the material interface, and an external electric circuit can be mounted on these surfaces to extract the DC.

2.2.2 Operation of solar module

Due to the small output voltage, the individual operation of a solar cell is a rare phenomenon, therefore; modules are used as basic building blocks. The series and parallel connections of the cells give convenient voltage.

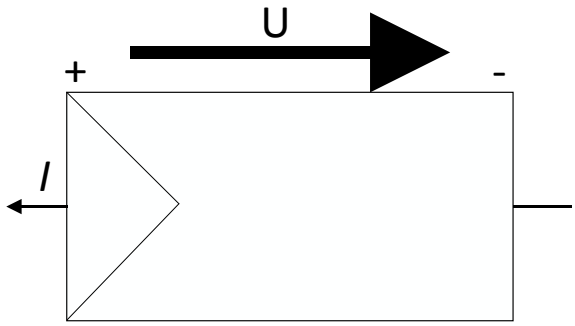

Figure 2.2. *Connection symbol of a solar module* ***[11]****.*

To achieve higher output voltage these PV modules are connected in series and for higher current ratings, in parallel or in both schemes for higher output power.

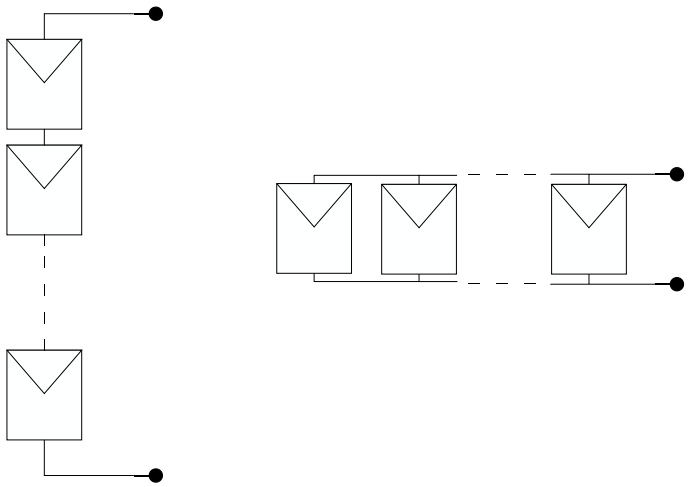

Figure 2.3. *Connections of solar modules* ***[11]****.*

2.3 Solar cell representation

Generally, a solar cell is represented using one-diode equivalent model having parasitic elements; series resistance R_s and shunt resistance R_{sh} and an ideal current source.

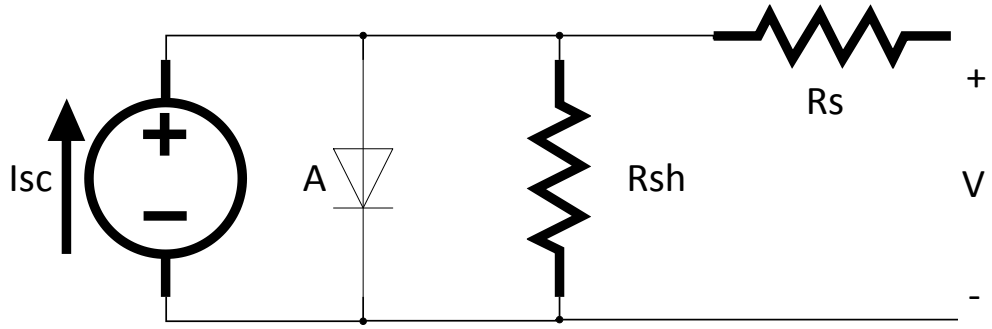

Figure 2.4. *Simplified one diode model for a solar cell.*

Figure 2.4 depicts the model for modeling the solar cell in *MATLAB,* where I_{sc} is the short-circuit current and V_{oc} is the open-circuit voltage produced by the solar cell.Parasitic elements; series and shunt resistances are used to represent the non-ideal behavior of a real solar cell and have the certain effect on the Current-Voltage (I-V) curve.

The commonly used equation to obtain the current produced by the solar cell is given below:

$$I = I_{sc} - I_o\left(e^{\frac{q(V+IR_S)}{akT}} - 1\right) - \frac{V+IR_S}{R_{sh}} \tag{2.1}$$

In above-mentioned equation I_o is the saturation current of the diode, a is the ideality factor, T is the temperature, k is Boltzman constant and q is the electron charge. The open-circuit voltage of the solar panel depends upon the short-circuit current and is given by:

$$V_{oc} = \frac{kT}{q}\ln\frac{I_{sc}+I_o}{I_o} \tag{2.2}$$

All the data sheets of PV panels are provided with V_{oc}, I_{sc}, voltage (V_{mp}) at maximum power point (MPP), the current (I_{mp}) at MPP, open circuit voltage/temperature coefficient (K_v), short circuit current/tamperature coefficient (K_i) and maximum peak

output power for experimentation ($P_{max,e}$). The following equations are used to obtain the values of series and shunt resistances by making $P_{max,m} = P_{max,e}$ [12]:

$$P_{max,m} = V_{mp}\left\{I_{pv} - I_o\left[exp\left(\frac{q}{kT}\frac{V_{mp}+R_sI_{mp}}{aN_s}\right) - 1\right] - \frac{V_{mp}+R_sI_{mp}}{R_p}\right\} \quad (2.3)$$

$$R_p = \frac{V_{mp}+R_sI_{mp}}{\left\{V_{mp}I_{pv} - V_{mp}I_o exp\left[\left(\frac{V_{mp}+R_sI_{mp}}{aN_s}\frac{q}{kT}\right)\right] + V_{mp}I_o - = P_{max,e}\right\}} \quad (2.4)$$

2.4 Electrical characteristics

The electrical characteristics of a PV cell are expressed by I-V curve and mainly two atmospheric factors affect solar panel's output; temperature and solar radiation. The irradiance has a linearised effect on short-circuit current which means increased in irradiance results in higher current output whereas the increment in temperature gives a little rise in current but open circuit voltage decreases significantly. Figure 2.5 and Figure 2.6 represent the electrical characteristics and effects of factors on the performance of PV panel.

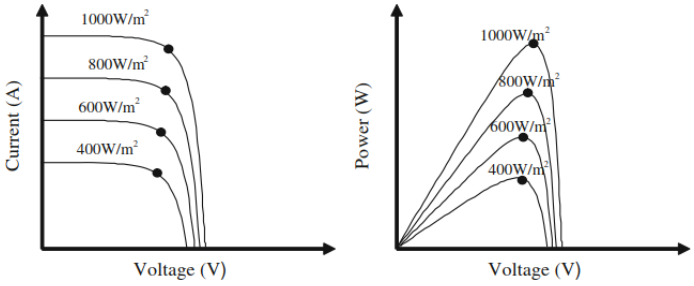

Figure 2.5. *Irradiance effect* ***[13]****.*

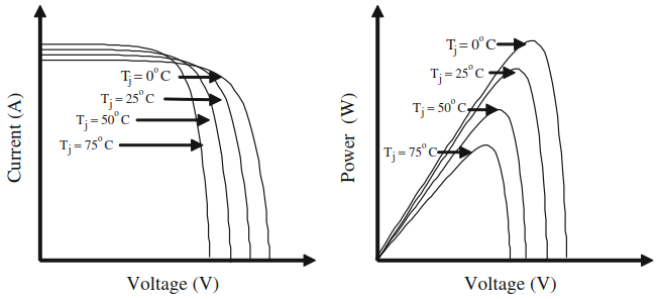

Figure 2.6. *Temperature effect* ***[13]****.*

As, electrical characteristics of the photovoltaic panel can be represented by the I-V curve and by using abovementioned equations (2.1) and (2.2) in *MATLAB,* I-V and Power Voltage (P-V) curves of a solar cell and panel are represented in Figure 2.7 and Figure 2.8 respectively.

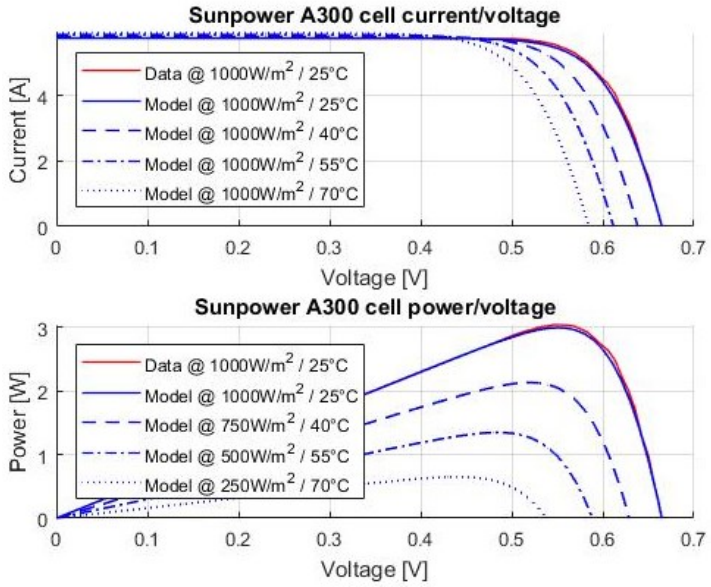

Figure 2.7. *Electrical characteristics of SUNPOWER A330 solar cell* ***[14].***

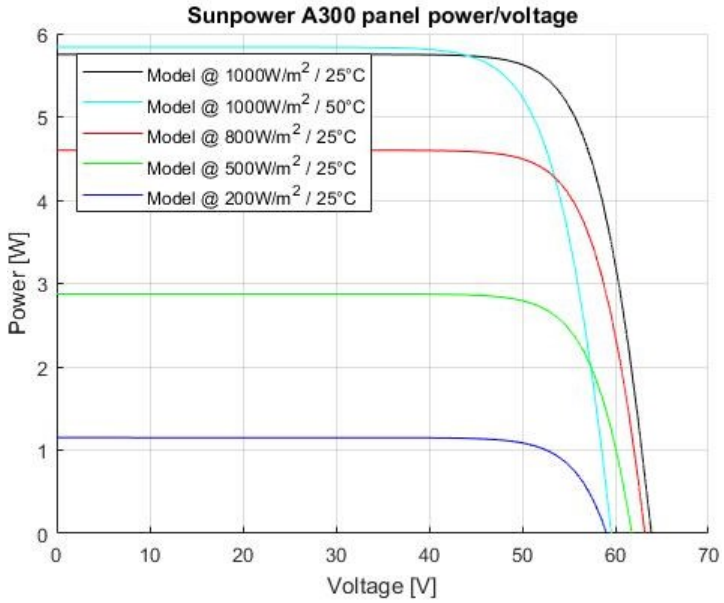

Figure 2.8. *P-V curve of Sunpower A330 panel* ***[14]****.*

2.4.1 Maximum power point tracking

As mentioned that output characteristics of the photovoltaic panel vary with varying irradiance and temperature so the design of the photovoltaic generator is a primary concern to track the MPP. A "*max*" command used to find the maximum power and "*val idx*" command to find the index where current and voltage were maximum to give MPP. Figure 2.9 shows the output power and electrical characteristics of the solar panel with MPP in per unit (p.u) value.

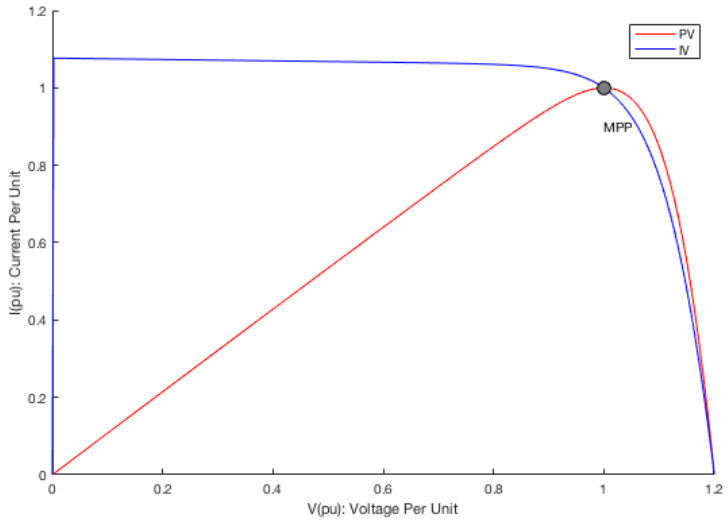

Figure 2.9. *IV and PV curve of SUNPOWER 220 with MPP.*

2.5 Classification of PV systems

Photovoltaic systems are designed by keeping in mind the definitive goal, like powering a small household or injecting power into electricity distribution grid. PV systems are categorized according to Figure 2.10.

Photovoltaic systems are mainly classified into stand-alone and grid-connected type PV systems. The defining factor of two classes is the load as in stand-alone systems the power from the solar panels matches the load demand whereas, in grid-connected type, the PV generator might produce and deliver excess energy to the electric grid or use electric grid as a substitute in case of incomplete power to match the load demand.

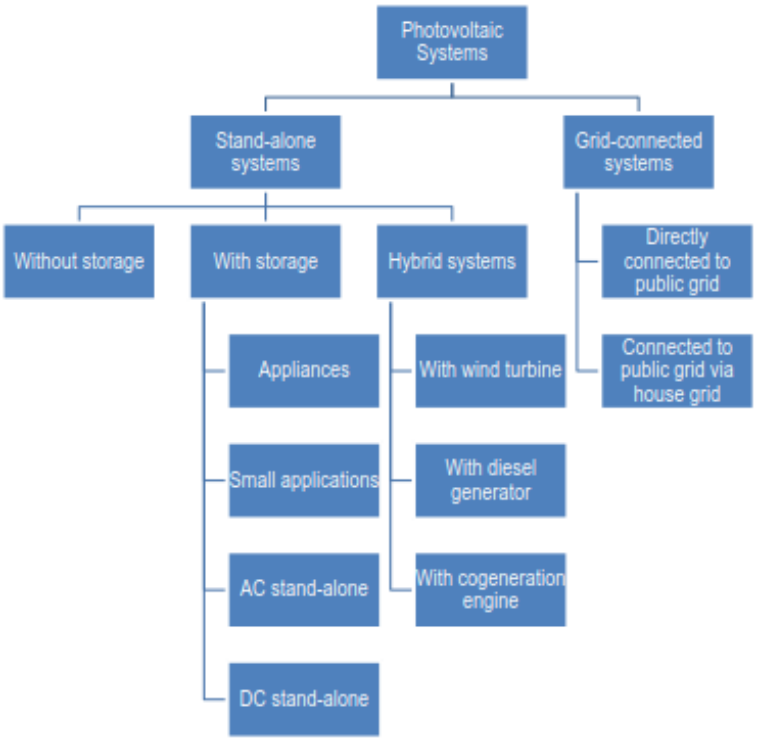

Figure 2.10. *Types of PV systems* ***[15]****.*

2.5.1 Stand-alone PV systems

Historically, the stand-alone systems were designed and used in rural areas where electricity distribution via utility grid was not applicable reason being the high cost of transmission lines and other distribution equipment. Recently, these systems are in practice for mobile communication, water heating and pumping applications. The stand-alone systems usually contain a solar generator, power control and storage unit and the load [16].

2.5.2 Grid connected PV systems

As discussed earlier the penetration of PV systems into the electricity network is on the rise and further expansion of grid-connected PV systems is expected as many countries around the globe are investing in the renewable energy and PV systems. The solar energy is set to surpass the nuclear energy by the end of 2017 and double by the end of 2022 [17]. The reason behind the grid-connected systems being advantageous is the facility to produce electricity near load points and thus reducing the cost of distribution and losses. These systems possess the bi-directional flow of the electricity, which means electric flow from, and to the utility grid is possible [16]. Figure 2.11and Figure 2.12 represent these two categories respectively.

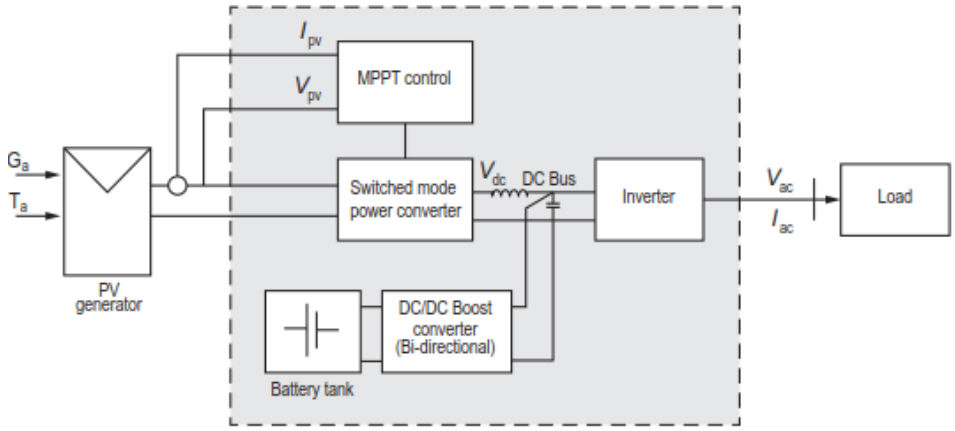

Figure 2.11. *Stand-alone PV system* ***[15]***.

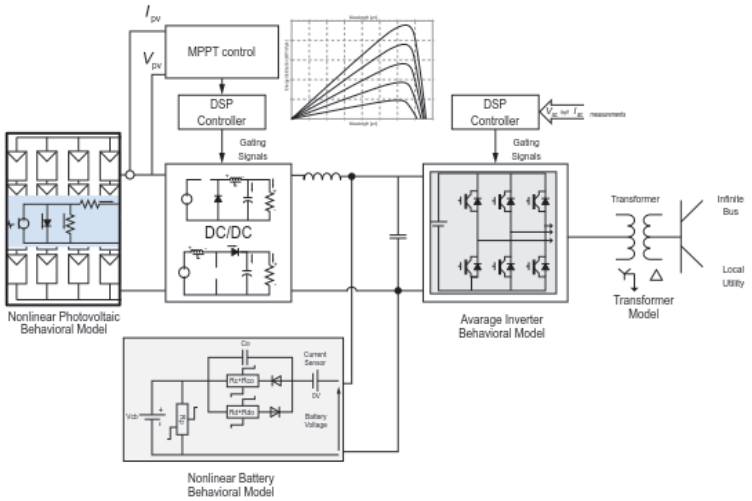

Figure 2.12. *Grid Connected PV system* ***[15]***.

2.6 Summary

This chapter gave a brief overview of the photovoltaic generator, its preferred usage approach to get the desired power and modeling in MATLAB by utilizing the one diode model with parasitic resistances. The electrical characteristics were presented by the means of I-V curve and voltage curve with the maximum power point. Moreover, two main classes of PV systems were discussed briefly. A simple photovoltaic model is used in this chapter, as this research thesis mainly focuses on the power flow assessment of the grid connected photovoltaic generator not the solar cell's properties under different atmospheric conditions. Chapter 4 gives the detailed presentation of the power flow algorithm.

3. POWER ELECTRONICS

3.1 Introduction

During recent years, power electronics applications have seen an increment in the usage of switched-mode converters [8]. As Figure 3.1 shows, in modern power systems, renewable energy resources perform the task of providing input to these DC-DC converters. To convert unregulated voltage into controlled DC voltage at the desired level, these converters are always first priority [18].

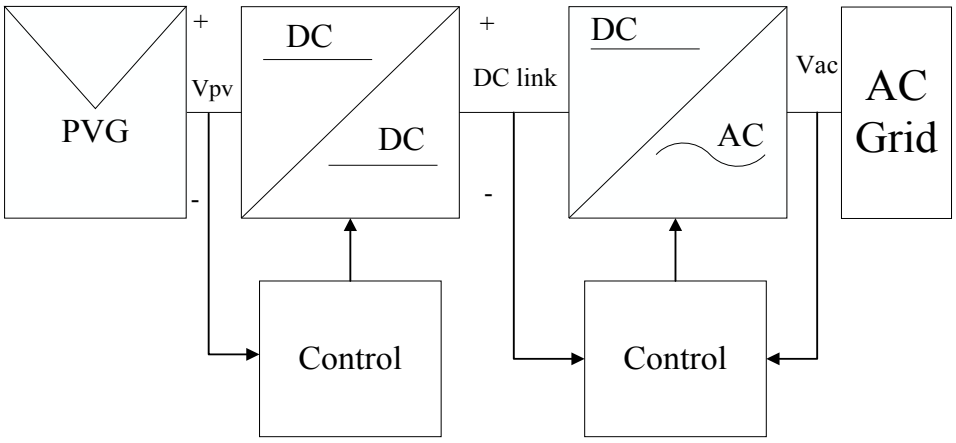

Figure 3.1. *Double stage grid connected PV generator.*

This chapter briefly discusses the basic working operations of DC-DC converters along with DC-AC converters. The essential concept to adopt these converters in power applications is to obtain a controlled and desired level of output voltage despite having fluctuations in input or load. This phenomenon is achieved by the means of switches having controlled *on* (t_{on}) and *off* (t_{off}) time. So total switching time is $T_s = t_{on} + t_{off}$.

3.1.1 Power switches

The *on* and *off* state of a power switch can be controlled via a control signal and this control capability defines the category of the switch i.e. Line commutated or self-commutated. To turn *on* the line-commutated switch, its gate must have a capable firing angle and the voltage across anode-cathode must be positive. These devices are referred by a single degree of freedom because they remain in conduction state until the current is zero and the negative voltage is established across anode-cathode. The most applicable switch

in this category is Silicon Controlled Rectifier (SCR) or thyristor [18]. The self-commutated switches offer more freedom as compared to others because they stop conducting once the control signal at the gate is removed. Insulated Gate Bipolar Transistor (IGBT), Gate Turn-Off thyristor (GTO) and Insulated Gate Commutated Thyristor (IGCT) fall into this category [18]. The Pulse Width Modulation (PWM) is popular scheme to enable this operation of switching at a fixed frequency. In this mode of operation, the duty ratio D describes the on and off time of the switch.

$$D = \frac{t_{on}}{T_s} \tag{3.1}$$

$$T_s = \frac{1}{f_s} \tag{3.2}$$

In equation (3.2), f_s is the switching frequency and opposite of total switching time.

3.2 DC-DC converters

3.2.1 Modes of operation

In steady-state operation, the operating mode of the converters could be defined with the analysis of inductor current. Fundamentally, there are three operating modes of a converter: continuous conduction mode (CCM), boundary conduction mode (BCM) and discontinuous conduction mode (DCM) [19]. When inductor current never touches the zero or remains greater than zero during the whole duty cycle, this mode of the converter is called CCM, whereas in DCM the inductor current remains zero or touches during some part of the duty cycle. In BCM, the inductor current goes to the zero at the end of a duty cycle. Figure 3.2 explains all these three modes of operation graphically.

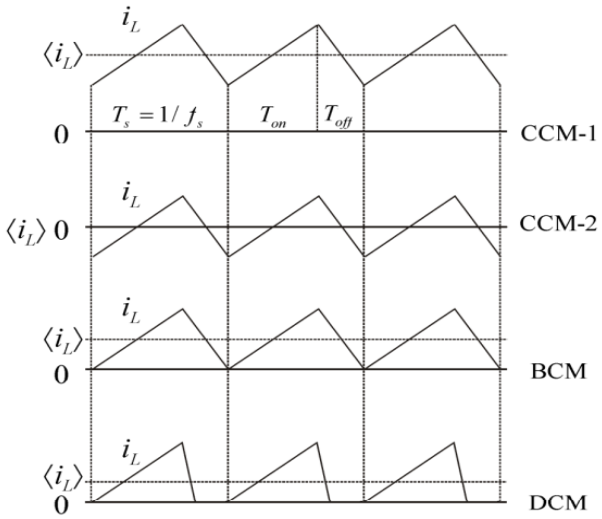

Figure 3.2 *Converters' conduction modes* ***[19]****.*

3.2.2 Buck Converter

The buck converter generates the desired level of output voltage but lower than input dc voltage, therefore it is also called the step-down converter. Control of dc motor speed is one of its applications. Figure 3.3 represents the buck converter schematically.

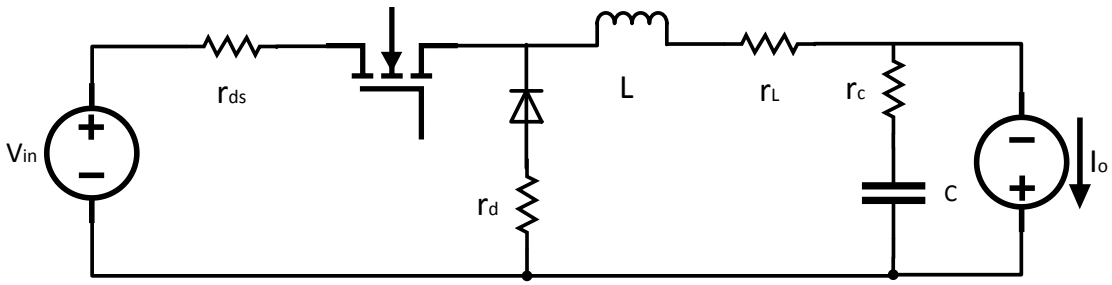

Figure 3.3. *Buck converter's schematic diagram* ***[19]****.*

Buck converters' mode of operation in CCM depends upon two states of the switch, *on* and *off*. In former operation, the switch is closed and the diode is reverse biased whereas in latter operation diode is forward biased because of the switch being in the open state. During *on* time, the input voltage gets its way to the inductor and load, whereas, in the *off* state, diode gets the inductor current due to energy being stored previously during the *on* state. Some part of this energy is also supplied to the load. Figure 3.4 and Figure 3.5 explain these two states.

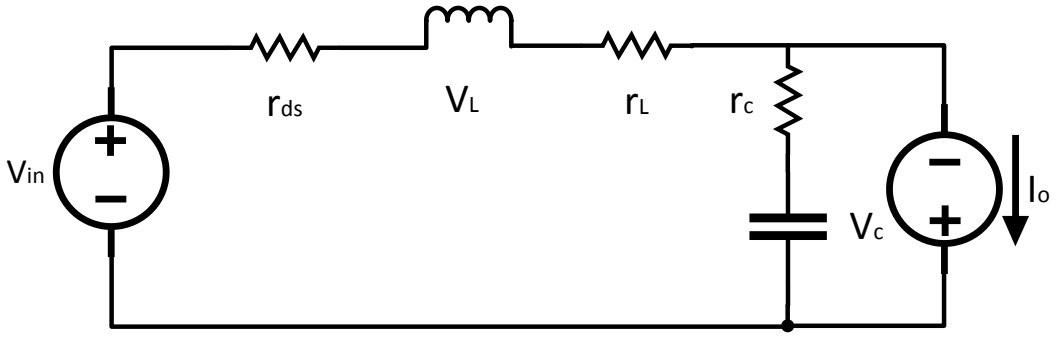

Figure 3.4. *On state of the buck converter.*

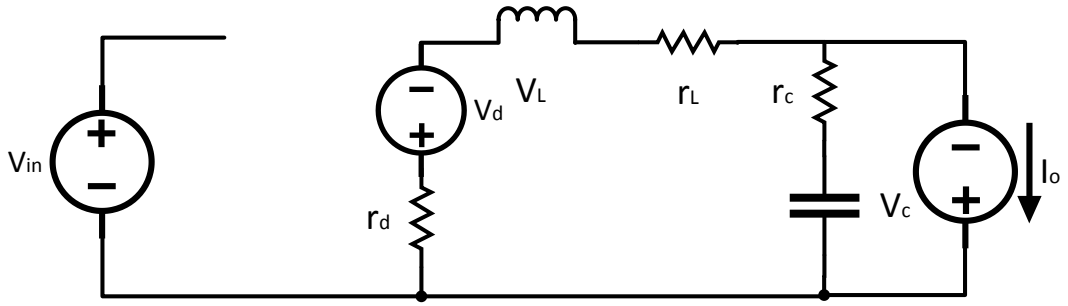

Figure 3.5. *Off state of the buck converter.*

3.2.3 Boost converter

Evident from the name, this converter produces output voltage larger than the input and called step-up converter too. Figure 3.6 represents the step-up converter.

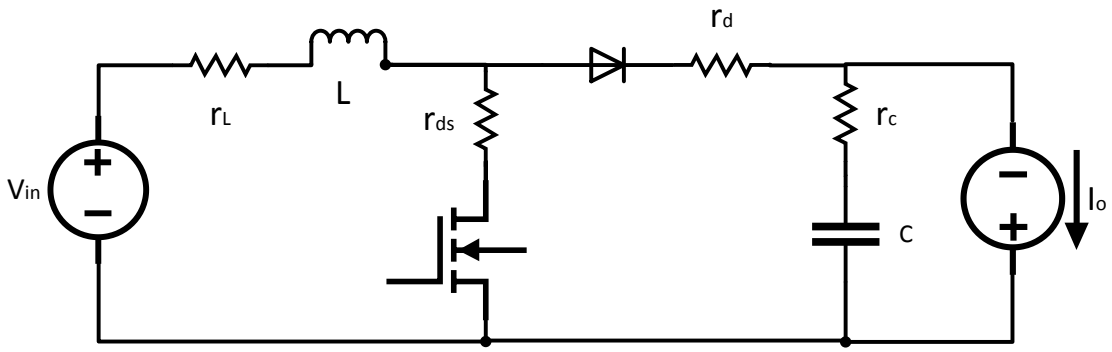

Figure 3.6. *Boost converter's schematic diagram* ***[19]****.*

The boost converter also operates in *on* and *off* states during CCM. The closing of the switch forces the diode to operate in the reverse bias mode, which results in disconnecting the output from the main circuit. During this whole time, the inductor receives and stores all the energy and gets fully charged. As the switch opens, the converter operates in the *off* state and the output circuit reconnects with input. Thus, output receives the input energy as well as the stored energy in the inductor. Figure 3.7 *and* Figure 3.8 graphically describe these two stages of the boost converter.

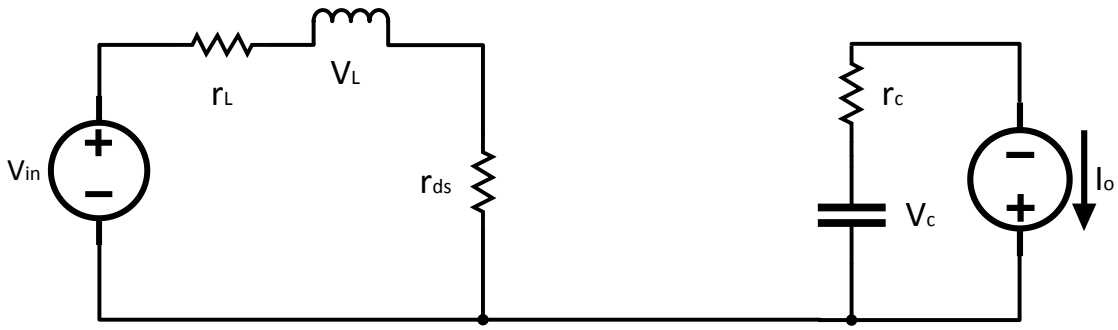

Figure 3.7. *On state of the boost converter.*

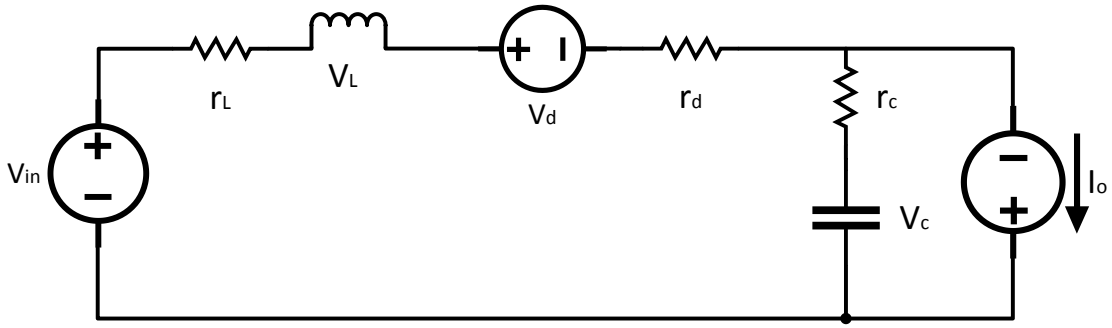

Figure 3.8. *Off state of the boost converter.*

3.2.4 Buck-Boost converter

A buck-boost converter is the cascaded connection of two basic step-down and step-up converters i.e. buck converter and boost converter. These converters are preferred in applications demanding negative polarity at the output [18]. This output could be higher or lower than the input according to the desired application's level. A basic buck-boost converter is represented in Figure 3.9.

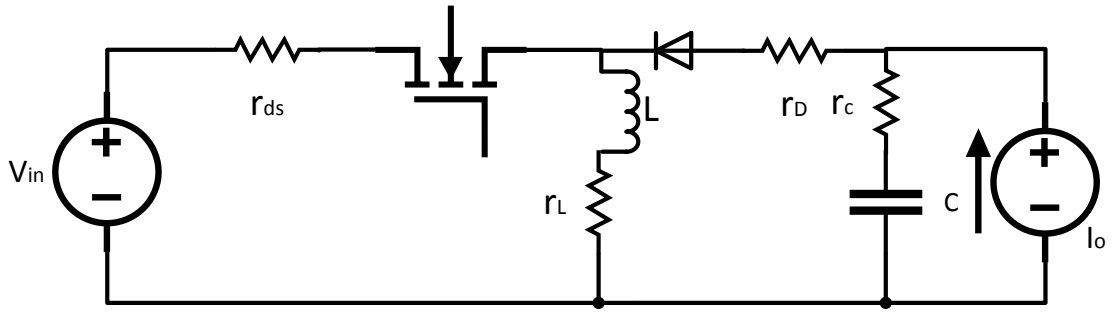

Figure 3.9. *Buck-boost converter's schematic diagram* ***[19]****.*

The *on* and *off* modes of operation related to buck-boost converter are as simple as previously discussed. During on time, when the switch is closed, the inductor gets charged due to receiving and storing all the input power. During this on time, the diode is reverse biased. As the switch changes its state from being close to open, the input circuit is insulated from the output and output receives the energy from the inductor stored during on time. Figure 3.9 Figure 3.10 and Figure 3.11 graphically explain these two stages of the buck-boost converter.

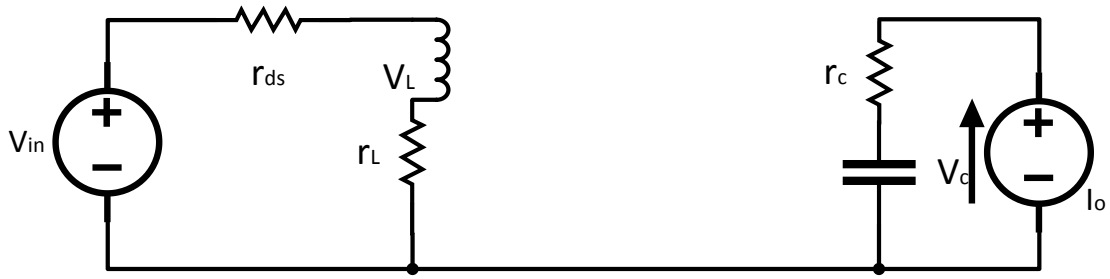

Figure 3.10. *On state of buck-boost converter.*

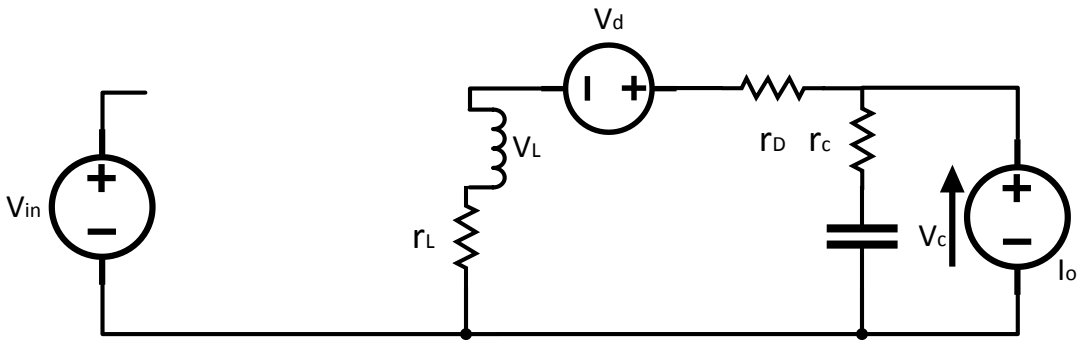

Figure 3.11. *Off state of buck-boost converter*

3.3 DC-AC converters

In a grid connected solar generator system, the DC-AC converter has the paramount importance and the basic responsibility of these devices is to convert DC power into AC and vice versa. These converters fall into two categories, VSC and Current Source Converter (CSC).

3.3.1 Current source converter

The CSC operates by using the thyristors to inject AC power into a DC system or vice versa. The operation of thyristors in this device limits its capability to one degree of freedom as discussed previously. Figure 3.12 presents the building block of CSC

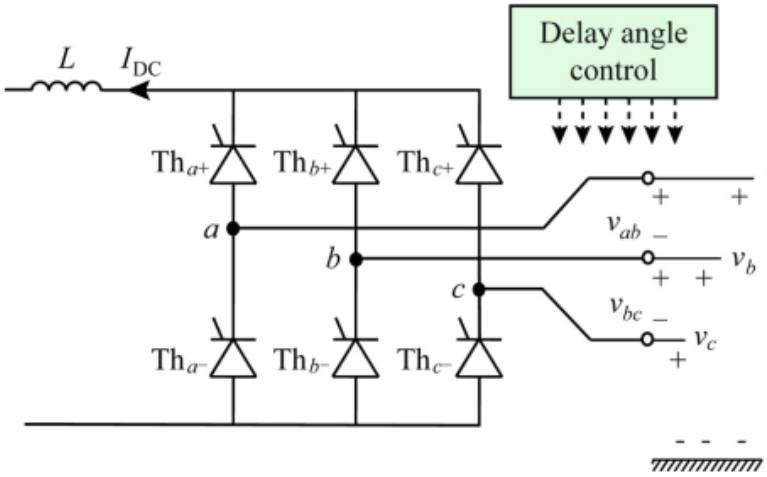

Figure 3.12. *AC/DC CSC* ***[20]****.*

3.3.2 Voltage source converter

The pivotal component of the *Flexible AC Transmission Systems* (FACTS) technology is Stator Compensator (STATCOM) and the fundamental configuration of STATCOM includes a VSC and a connecting transformer, which is most often load tap changing (LTC) [21] [22]. The VSC operates by using the IGBTs to inject AC power into a DC system or vice versa. The operation of IGBTs with freewheeling diodes in this device allows the full degree of freedom. Figure 3.13 represents the schematic diagram of VSC.

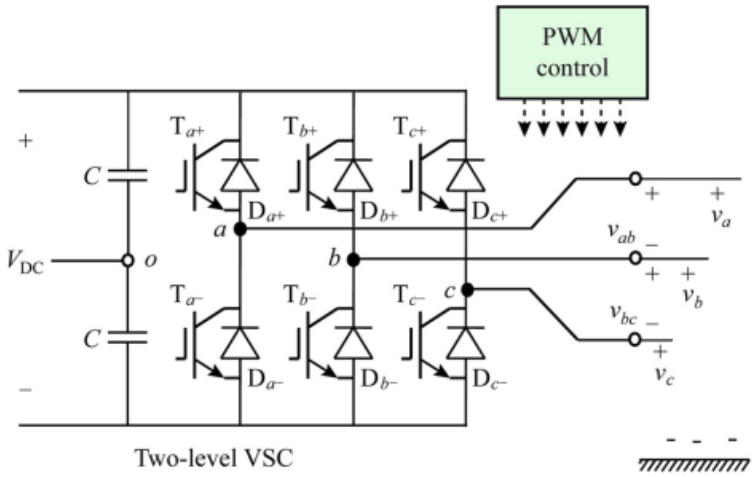

Figure 3.13. *Two level VSC* ***[20]****.*

The power switches or IGBTs in the configuration of this device are controlled via PWM signals and the capacitor on its DC side acts as a voltage source. As illustrated in Figure

3.14, this control scheme synthetizes the fundamental frequency voltage on AC side from DC bus [20].

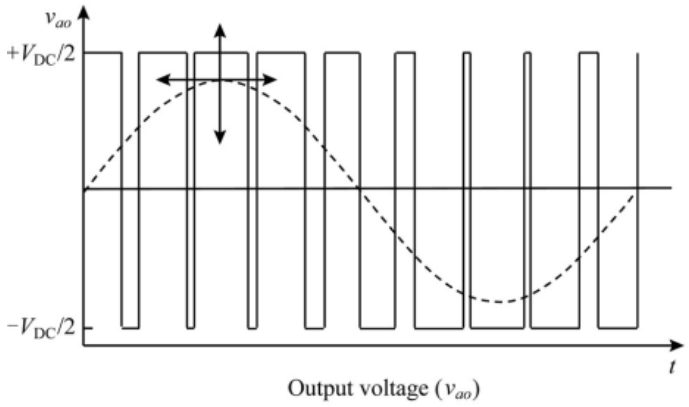

Figure 3.14. *PWM performance* ***[20]****.*

The reason for Voltage Source Converters being self-commutated is that they offer better power control and flexibility as compared to CSCs, by working with fully controlled power electronics [23] [24]. The operation of self-commutated VSCs is spread in all four quadrants of the P-Q plane as they offer bi-directional active and reactive power flow in AC side alongside bi-directional active power flow in DC side [25]. Two main factors affect the control of the active and reactive power between VSC and electric power system; phase angle and converter's voltage magnitude [23]. Figure 3.15 and Figure 3.16 represent the VSC schematic diagram and its equivalent circuit respectively, which is being used in this research thesis [26].

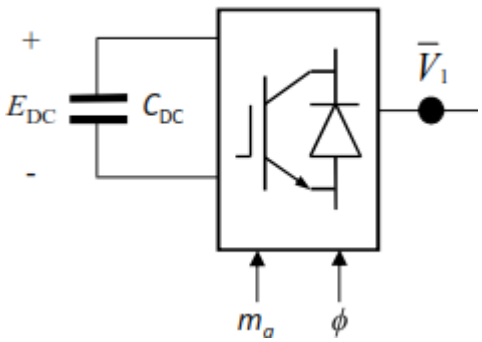

Figure 3.15. *VSC schematic representation* ***[27]****.*

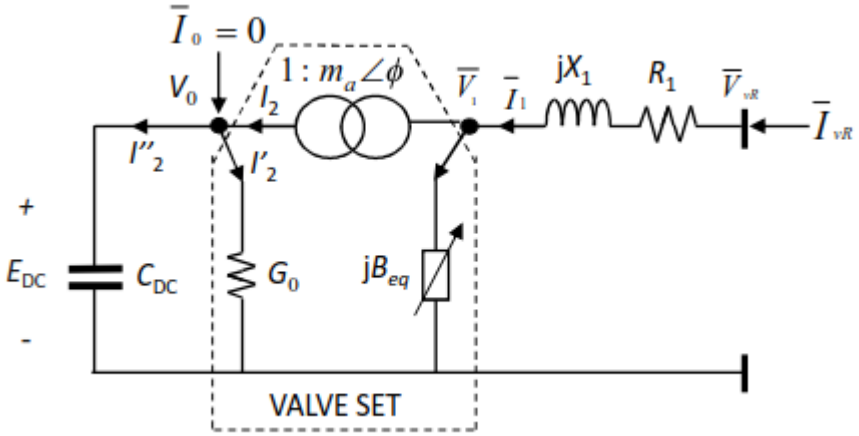

Figure 3.16. *VSC equivalent circuit* ***[27]****.*

Practically, the design of a VSC can be a two-level or multi-level, which is operated by IGBTs, controlled by PWM. The capacitor bank on the DC side of the VSC has a small rating, which has an exclusive objective of stabilizing the DC voltage to make VSC operate properly. The converter makes the capacitor's voltage lag the AC system by a small angle in order to maintain a required capacitor voltage [22]. It should be noted that VAR generation and absorption process is not the responsibility of the capacitor instead; this step is carried out by PWM control [28]. The basic relationship is given below:

$$\bar{V}_1 = K_1 m_a e^{j\phi} E_{DC} \tag{3.3}$$

The complex voltage $\bar{V}_1$ is relative to system phase reference, m_a is the tap magnitude of ideal phase shifting transformer which is related to amplitude modulation of the VSC, ϕ is the phase angle of the voltage, E_{DC} is the scaler value of the DC bus and $K_1 = \sqrt{\frac{3}{8}}$ for two level, three phase VSC [28]. As we can see from Figure 3.16 a VSC consist of an ideal phase shifting transformer, its equivalent shunt susceptance is donated by B_{eq}, series reactance by jX, whereas, the series resistor is related with ohmic losses. The mathematical modeling of VSC is presented in Chapter 4.

3.3.3 Converters' topology

The above-mentioned converters are built in self-commutated or line-commutated topology. Self-commutated converters possess the qualities of both VSCs and CSCs as compared to line-commutated, which can only act as CSCs [22]. Figure 3.17, Figure 3.18 and Figure 3.19 present the classification of power converters [29].

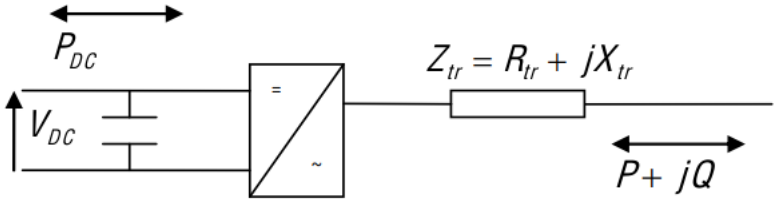

Figure 3.17 *Self-commutated VSC.*

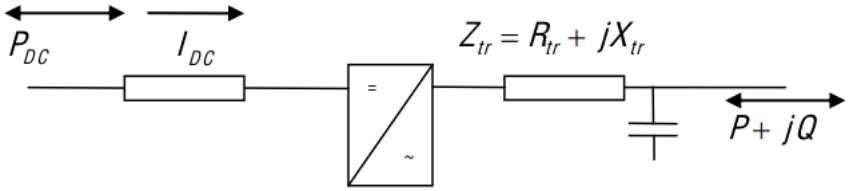

Figure 3.18 *Self-commutated CSC.*

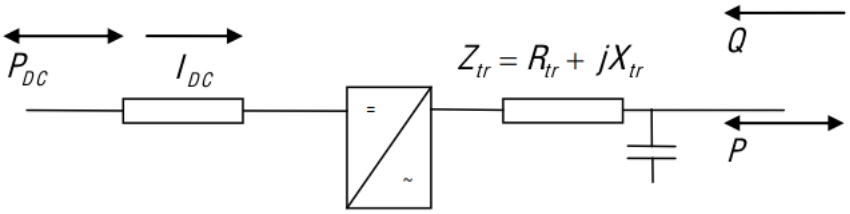

Figure 3.19 *Line-commutated CSC.*

From Figure 3.17, we can see that VSC owns a DC voltage power supply whose polarity never changes irrespective of the circuit and is most often a capacitor so the changes in the direction of DC current directly affect the flow of the power from or to the converter [22] [30].

3.4 Summary

In this chapter, basic DC-DC, DC-AC converters were briefly discussed. Moreover, their control and modes of operation were represented. As the buck-boost converter and VSC is being used in this research thesis so the mathematical modeling; which includes constructing the admittance matrix, obtaining nodal power equations and building Jacobian matrix is represented in the Chapter 4 which elaborate the power flows.

4. POWER FLOWS

4.1 Introduction

The electrical power networks have seen an extensive revolution in recent years, so the smooth flow of electricity is an enormous challenge [22]. In this endeavour, Narain G. Hingorani and Lazlo Gygui cannot be forgotten for pioneering the new technology, (FACTS) and this chapter provides the explanation about the flow of smooth electricity in electric power systems by utilizing mathematical approach in power flows. The power flow algorithm is solved by the means of Newton Raphson method because it is robust and converges fast.

4.2 Power flows

The fundamental goal of power flows studies is to analyse the condition of an electric power network under steady-state operation by assessing its voltage magnitudes, phase angles, nodal active and reactive powers and transmission line power flows [21].

4.2.1 Representation in power flows

Some common representations are used to represent a set of identities in power flow studies, given below:

- The *buses* commonly used in power system studies, represent bus-bars
- There are positive and negative power injections points in an electric power network. The former represents synchronous generators whereas the later serves as the load, which could depend on voltage.
- Transmission lines are modelled as nominal *pi* circuits and tap changing transformers as equivalent *pi* circuits.
- Series impedances represent the power transformers
- Series capacitors are modelled as series capacitive reactance.
- Shunt reactors and capacitor banks could be modelled as either shunt inductive or capacitive reactance.

4.2.2 Types of buses

There are four quantities; active and reactive power, voltage magnitude and angle, associated with each bus that thoroughly determines the state of an electric grid. In conventional power flows, there are three types of buses [30], having known and unknown information, explained below:

1. *Slack or* the *swing* bus serves as the reference for all the calculations. The voltage angles of other buses are calculated by taking the voltage angle of the slack bus as a reference.
2. The *Generator* bus is that bus of the system where voltage magnitude is known and kept constant. This bus is called PV-bus. The reactive power and voltage angle are the unknowns at this bus and thus should be calculated
3. The *Load* bus is also called PQ-bus and has no generator. As it is a load bus so active and reactive power consumptions are the known values and voltage magnitude and angle are calculated.

The table given below outlines the types and related quantities of buses.

Table 4.1. *Types of buses in power flows.*

Bus type	**Known**	**Calculated**
Slack or swing	V and θ	P and Q
Generator or PV	V and P	Q and θ
Load or PQ	P and Q	V and θ

4.3 Iterative solution

From the vantage of mathematical modelling of the electric power networks, the optimal power flow aims at solving non-linear, algebraic equations and to carry out this exercise, the ***Newton-Raphson*** method overcame other numerical techniques [30]. The main purpose of the NR method [31] is to approximate the solution of a non-linear function $F(x) = 0$ for x using first two terms of Taylor series expansion. If supposed $x^{(i)}$ is the guessed solution of $F(x)$ at iteration i then equation (4.1) explains its expansion.

$$F(x^{(i)}) = F(x^{(i-1)}) + F'(x^{(i-1)})\Delta x^{(i)} \tag{4.1}$$

Solving equation (4.1) yields the linear equation (4.2):

$$F(x^{(i-1)}) = -F'(x^{(i-1)})\Delta x^{(i)} \tag{4.2}$$

From equation (4.2):

$$\Delta x^{(i)} = -F'(x^{(i-1)})^{-1} F(x^{(i-1)}) \tag{4.3}$$

From (4.3) the initial guessed approximation of linearized equations will be updated using mismatch $\Delta x^{(i)}$. Once the function is smaller than the tolerance level, the solution stops.

To work with NR method in electric power flows, it must be equipped with applicable nodal active and reactive power flow equations, which can be derived from the complex power injection equation at a *node* l [30], given below:

$$S_l = P_l + jQ_l = V_l I_l^* \tag{4.4}$$

In equation (4.4):

Subscript l indicates the node of the system,

S_l is the complex power injection at node l,

P_l and Q_l are active and reactive power, respectively, entering node l,

$j = \sqrt{-1}$ and * indicate the complex conjugate.

The current injected at node l represents the sum of all the currents in n branches connected with node l:

$$I_l = I_{l1} + \ldots + I_{lk} + \ldots + I_{ln} \tag{4.5}$$

$$I_l = \sum_{m=1}^{n} I_{lm} \tag{4.6}$$

According to *Ohm's* Law, the equation (3.6) becomes,

$$I_l = \sum_{m=1}^{n} Y_{lm} V_m \tag{4.7}$$

In equation (3.7), the admittance Y_{lm} is the sum of conductance G_{lm} and susceptance B_{lm} of the branches $l - m$.

By putting the value of I_l from equation (4.7) into equation (4.4), we get the below given result:

$$P_l + jQ_l = V_l \sum_{m=1}^{n} Y_{lm}^* V_m^* \tag{4.8}$$

Expressing the voltages in equation (3.8), in polar co-ordinates:

$$P_l + jQ_l = V_l e^{j\theta_l} \sum_{m=1}^{n} \left(G_{lm} - jB_{lm}\right) V_m e^{j\theta_m} \tag{4.9}$$

From equation (4.9) nodal active and reactive power equations are obtained by the means of the product of complex numbers:

$$P_l = V_l \sum_{m=1}^{n} V_m \{G_{lm} \cos(\theta_l - \theta_m) + B_{lm} \sin(\theta_l - \theta_m)\} \tag{4.10}$$

$$Q_l = V_l \sum_{m=1}^{n} V_m \{G_{lm} \sin(\theta_l - \theta_m) - B_{lm} \cos(\theta_l - \theta_m)\} \tag{4.11}$$

Where V_l and V_m are the magnitudes of the nodal voltages and θ_l and θ_m are the phase angles at the nodes.

From these equations, a steady state analysis of a power network is possible but due to the non-linear nature, they require an iteration method: Newton Raphson, as explained earlier. As electric buses explained earlier, this method takes two variables as specified and other two unknowns are calculated.

The Newton Raphson method gives the solution of equations (4.10) and (4.11) but it needs a set of linearized equations (4.12), which demonstrates the relationship of changes and developments of the whole system's variables, excluding the *slack* bus.

$$\begin{bmatrix} \Delta P_2 \\ \Delta P_3 \\ \vdots \\ \Delta P_n \\ \Delta Q_2 \\ \Delta Q_3 \\ \vdots \\ \Delta Q_n \end{bmatrix}^r = \begin{bmatrix} \partial P_2/\partial\theta_2 & \partial P_2/\partial\theta_3 & \cdots & \partial P_2/\partial\theta_n & (\partial P_2/\partial V_2)V_2 & (\partial P_2/\partial V_3)V_3 & \cdots & (\partial P_2/\partial V_n)V_n \\ \partial P_3/\partial\theta_2 & \partial P_3/\partial\theta_3 & \cdots & \partial P_3/\partial\theta_n & (\partial P_3/\partial V_2)V_2 & (\partial P_3/\partial V_3)V_3 & \cdots & (\partial P_3/\partial V_n)V_n \\ \vdots & \vdots & \ddots & \vdots & \vdots & \vdots & \ddots & \vdots \\ \partial P_n/\partial\theta_2 & \partial P_n/\partial\theta_3 & \cdots & \partial P_n/\partial\theta_n & (\partial P_n/\partial V_2)V_2 & (\partial P_n/\partial V_3)V_3 & \cdots & (\partial P_n/\partial V_n)V_n \\ \partial Q_2/\partial\theta_2 & \partial Q_2/\partial\theta_3 & \cdots & \partial Q_2/\partial\theta_n & (\partial Q_2/\partial V_2)V_2 & (\partial Q_2/\partial V_3)V_3 & \cdots & (\partial Q_2/\partial V_n)V_n \\ \partial Q_3/\partial\theta_2 & \partial Q_3/\partial\theta_3 & \cdots & \partial Q_3/\partial\theta_n & (\partial Q_3/\partial V_2)V_2 & (\partial Q_3/\partial V_3)V_3 & \cdots & (\partial Q_3/\partial V_n)V_n \\ \vdots & \vdots & \ddots & \vdots & \vdots & \vdots & \ddots & \vdots \\ \partial Q_n/\partial\theta_2 & \partial Q_n/\partial\theta_3 & \cdots & \partial Q_n/\partial\theta_n & (\partial Q_n/\partial V_2)V_2 & (\partial Q_n/\partial V_3)V_3 & \cdots & (\partial Q_n/\partial V_n)V_n \end{bmatrix}^r \begin{bmatrix} \Delta\theta_2 \\ \Delta\theta_3 \\ \vdots \\ \Delta\theta_n \\ \Delta V_2/V_2 \\ \Delta V_3/V_3 \\ \vdots \\ \Delta V_n/V_n \end{bmatrix}^r \tag{4.12}$$

In (4.12), the active or reactive power mismatch at any node l is the difference between net scheduled and calculated powers as mentioned below:

$$\Delta P_l = P_l^{net} - P_l^{calc},$$

$$\Delta Q_l = Q_l^{net} - Q_l^{calc},$$

where:

$$P_l^{net} = P_l^{gen} - P_l^{load},$$

$$Q_l^{net} = Q_l^{gen} - Q_l^{load},$$

The superscripts *gen* and *load* give the information about the generated or consumed powers, respectively, at node l, whereas; (r) represents the iteration number. In (4.12), the matrix of first-order partial derivative terms are referred to the Jacobian matrix and to make it simpler the Jacobian elements of multiplication of voltage magnitude with voltage magnitudes [32]. The Jacobian matrix is recalculated at the end of each iteration"r". The elements of the Jacobian matrix when $l = m$, also called self-Jacobian, is given below:

$$\frac{\partial P_l}{\partial \theta_l} = V_l \sum_{m=1}^{n} V_m \{-G_{lm} \sin(\theta_l - \theta_m) + B_{lm} \cos(\theta_l - \theta_m)\} - V_l^2 B_{ll} = -Q_l - V_l^2 B_{ll} \quad (4.13)$$

$$\frac{\partial P_l}{\partial V_l} V_l = V_l \sum_{m=1}^{n} V_m \{G_{lm} \cos(\theta_l - \theta_m) + B_{lm} \sin(\theta_l - \theta_m)\} + V_l^2 G_{ll} = P_l + V_l^2 G_{ll} \quad (4.14)$$

$$\frac{\partial Q_l}{\partial \theta_l} = V_l \sum_{m=1}^{n} V_m \{G_{lm} \cos(\theta_l - \theta_m) + B_{lm} \sin(\theta_l - \theta_m)\} - V_l^2 G_{ll} = P_l - V_l^2 G_{ll} \quad (4.15)$$

$$\frac{\partial Q_l}{\partial V_l} V_l = V_l \sum_{m=1}^{n} V_m \{G_{lm} \sin(\theta_l - \theta_m) - B_{lm} \cos(\theta_l - \theta_m)\} - V_l^2 B_{ll} = Q_l - V_l^2 B_{ll} \quad (4.16)$$

In case of $l \neq m$, also termed as mutual-Jacobian elements:

$$\frac{\partial P_l}{\partial \theta_m} = V_l V_m \{G_{lm} \sin(\theta_l - \theta_m) - B_{lm} \cos(\theta_l - \theta_m)\} \quad (4.17)$$

$$\frac{\partial P_l}{\partial V_m} V_m = V_l V_m \{G_{lm} \cos(\theta_l - \theta_m) + B_{lm} \sin(\theta_l - \theta_m)\} \quad (4.18)$$

$$\frac{\partial Q_l}{\partial \theta_m} = -V_l V_m \{G_{lm} \cos(\theta_l - \theta_m) + B_{lm} \sin(\theta_l - \theta_m)\} \quad (4.19)$$

$$\frac{\partial Q_l}{\partial V_m} V_m = V_l V_m \{G_{lm} \sin(\theta_l - \theta_m) - B_{lm} \cos(\theta_l - \theta_m)\} \quad (4.20)$$

In order to run the iterative solution, it must be provided with the initial estimates for all the variables to determine the active and reactive powers using equations (4.10-4.11). As these initial estimates would not agree with the correct values, so mismatch power vectors are given below:

$$\Delta P^{(r)} = (P^{gen} - P^{load}) - P^{calc,(r)} = P^{net} - P^{calc,(r)} \quad (4.21)$$

$$\Delta Q^{(r)} = (Q^{gen} - Q^{load}) - Q^{calc,(r)} = Q^{net} - Q^{calc,(r)} \quad (4.22)$$

After calculating the Jacobian elements, the linearized set of equations (4.12) is solved to attain the voltage updates vector, given below:

$$\theta^{(r)} = \theta^{(r-1)} + \Delta\theta^{(r)} \tag{4.23}$$

$$V^{(r)} = V^{(r-1)} + (\Delta V/V)^{r}.V^{(r-1)} \tag{4.24}$$

The active and reactive power, a linearized set of equations, power mismatches and voltage updates are repeatedly evaluated in a sequence until the power mismatches are within a tolerance which is normally set to $\epsilon = 10^{-12}$.

4.4 Newton-Raphson flow diagram

The primary reasons for selecting the Newton-Raphson method as the iterative solution to evaluate a power network; are rapid convergence and better reliability, however, it is fair to say that the reliability of this method is largely dependent upon initial estimates which could result in unwanted complications if not chosen correctly [29]. Figure 4.1 summarises the Newton-Raphson method in a flow diagram.

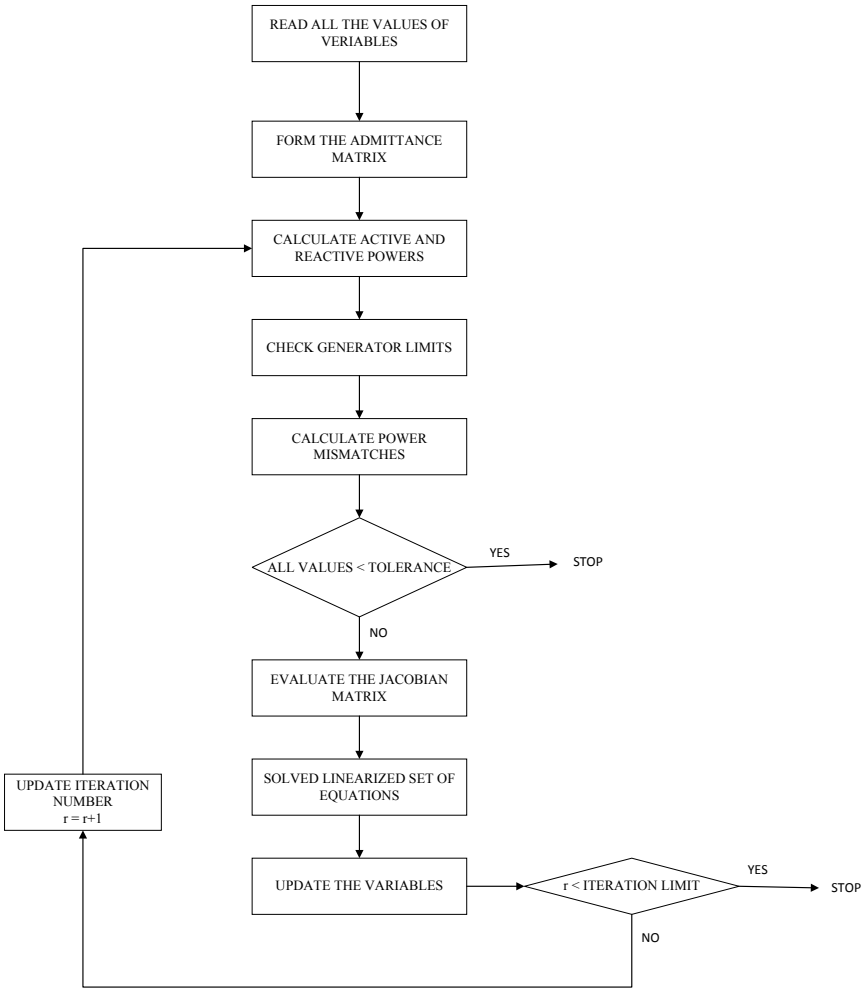

Figure 4.1. *Newton-Raphson power flow algorithm.*

4.5 VSC modeling

Power converters play a critical role in present-day electricity networks. The next important step in this research thesis is to understand the operating principles of VSC. Figure 4.2 represents the schematic diagram of VSC [26].

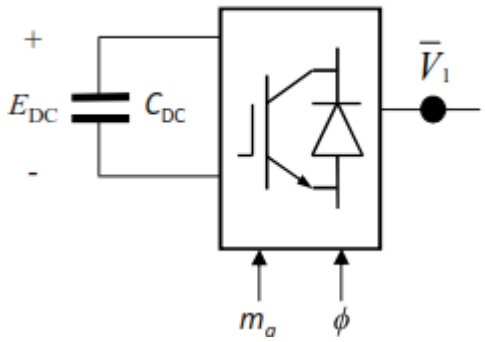

Figure 4.2. *Schematic diagram of VSC* ***[27]****.*

Where:

$$\bar{V}_1 = K_1 m_a e^{j\phi} E_{DC} \tag{4.25}$$

Figure 4.3 represents the equivalent circuit of VSC.

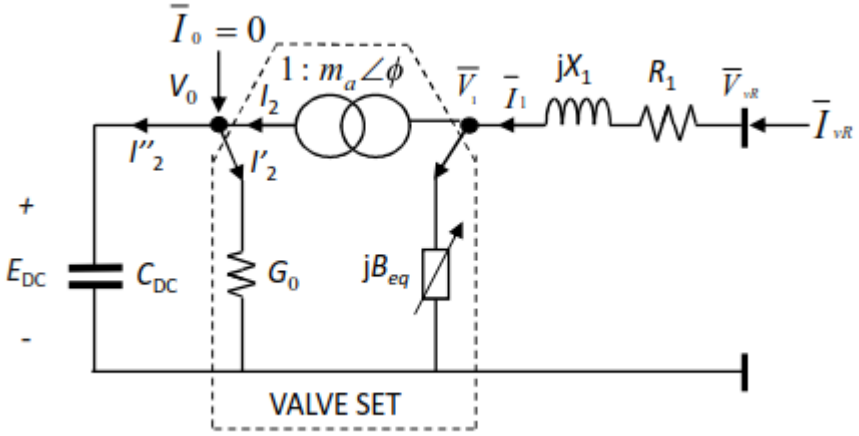

Figure 4.3. *VSC equivalent circuit* ***[27]****.*

Where:

$$V_o I_2 = \mathrm{Re}(\bar{V}_1 \bar{I}^*_1) \tag{4.26}$$

$$V_o I_2 = \bar{V}_1 (\bar{I}^*_1 - \bar{I}^*_1) = \bar{V}_1 \bar{I}^*_1 + jB_{eq} V_1^2 \tag{4.27}$$

$$G_o.\left(\frac{I_2^{nom}}{I_2^{nom}}\right)^2 \Rightarrow G_{sw} \tag{4.28}$$

$$\begin{pmatrix} \bar{I}_{vR} \\ \bar{I}_o = 0 \end{pmatrix} = \begin{pmatrix} \overline{Y_1} & -K_1 m_a(\cos\varphi + j\sin\varphi)\overline{Y_1} \\ -K_1 m_a(\cos\varphi - j\sin\varphi)\overline{Y_1} & G_{sw}+K_1{}^2 m_a{}^2(\overline{Y_1} + jB_{eq}) \end{pmatrix}\begin{pmatrix} \overline{V}_{vR} \\ V_o \end{pmatrix} \tag{4.29}$$

As complex power is:

$$\begin{pmatrix} \bar{S}_{vR} \\ \bar{S}_o \end{pmatrix} = \begin{pmatrix} \overline{V}_{vR} & 0 \\ 0 & V_o \end{pmatrix}\begin{pmatrix} \overline{I_{vR}^*} \\ \overline{I^*}_o \end{pmatrix} \tag{4.30}$$

From equation (4.29):

$$\begin{pmatrix} \bar{S}_{vR} \\ \bar{S}_o \end{pmatrix} = \begin{pmatrix} \overline{V}_{vR} & 0 \\ 0 & V_o \end{pmatrix}\left\{\begin{pmatrix} \overline{Y_1}^* & -K_1 m_a(\cos\varphi + j\sin\varphi)\overline{Y_1}^* \\ -K_1 m_a(\cos\varphi - j\sin\varphi)\overline{Y_1}^* & G_{sw}+K_1{}^2 m_a{}^2(\overline{Y_1}^* + jB_{eq}) \end{pmatrix}\begin{pmatrix} \overline{V_{vR}}^* \\ V_o \end{pmatrix}\right\} \tag{4.31}$$

Following some complex algebra, nodal active and reactive powers equations at sending and receiving node arrived as given below:

$$P_{vR} = G_1 V_{vR}^2 - K_1 m_a V_{vR} V_o\left[G_1\cos(\theta_{vR} - \theta_o - \varphi) + B_1\sin(\theta_{vR} - \theta_o - \varphi)\right]$$

$$Q_{vR} = -B_1 V_{vR}^2 - K_1 m_a V_{vR} V_o\left[G_1\sin(\theta_{vR} - \theta_o - \varphi) - B_1\cos(\theta_{vR} - \theta_o - \varphi)\right]$$

$$P_o = (K_1{}^2 m_a{}^2 G_1 + G_{sw})V_o^2 - K_1 m_a V_{vR} V_o\left[G_1\cos(\theta_o - \theta_{vR} + \varphi) + B_1\sin(\theta_o - \theta_{vR} + \varphi)\right]$$

$$Q_o = -K_1{}^2 m_a{}^2(B_1 + B_{eq})V_o^2 - K_1 m_a V_{vR} V_o\left[G_1\sin(\theta_o - \theta_{vR} + \varphi) - B_1\cos(\theta_o - \theta_{vR} + \varphi)\right] \tag{4.32}$$

From above calculated nodal power equations, the linearized system of equations is defined as:

$$\begin{bmatrix} \Delta P_{vR} \\ \Delta Q_{vR} \\ \Delta P_o \\ \Delta Q_o \\ \Delta P_{o-vr} \\ \Delta Q_{o-vr} \end{bmatrix} = \begin{bmatrix} \partial P_{vR}/\partial\theta_{vR} & (\partial P_{vR}/\partial m_a)m_a & \partial P_{vR}/\partial\theta_o & 0 & \partial P_{vR}/\partial\varphi & \partial P_{vR}/\partial B_{eq} \\ \partial Q_{vR}/\partial\theta_{vR} & (\partial Q_{vR}/\partial m_a)m_a & \partial Q_{vR}/\partial\theta_o & 0 & \partial Q_{vR}/\partial\varphi & \partial Q_{vR}/\partial B_{eq} \\ \partial P_o/\partial\theta_{vR} & (\partial P_o/\partial m_a)m_a & \partial P_o/\partial\theta_o & 0 & \partial P_o/\partial\varphi & \partial P_o/\partial B_{eq} \\ 0 & 0 & 0 & 1 & 0 & 0 \\ \Delta P_{o-vr}/\partial\theta_{vR} & (\Delta P_{o-vr}/\partial m_a)m_a & \Delta P_{o-vr}/\partial\theta_o & 0 & \Delta P_{o-vr}/\partial\varphi & \Delta P_{o-vr}/\partial B_{eq} \\ \Delta Q_{o-vr}/\partial\theta_{vR} & (\Delta Q_{o-vr}/\partial m_a)m_a & \Delta Q_{o-vr}/\partial\theta_o & 0 & \Delta Q_{o-vr}/\partial\varphi & \Delta Q_{o-vr}/\partial B_{eq} \end{bmatrix} \times \begin{bmatrix} \Delta\theta_{vR} \\ \Delta m_a/m_a \\ \Delta\theta_o \\ \Delta V_o/V_o \\ \Delta\varphi \\ \Delta B_{eq} \end{bmatrix} \tag{4.33}$$

In a voltage source converter, active and reactive powers between DC and AC side are controlled by phase sifting angle [33]. The VSC is capable of providing four control capabilities mentioned below in the table.

Table 4.2. *VSC modes of operation* ***[29]****.*

Mode of operation	**Control state**
No control	0
Voltage control	1
Power control	2
Both voltage and power control	3

4.6 Buck-boost converter modeling

The mathematical modeling of the buck-boost converter; which includes constructing the admittance matrix, obtaining nodal power equations and building Jacobian matrix, can be carried out by analyzing the performance of the converter in steady state conditions. According to [18], the lossless buck-boost converter circuit yields:

$$\frac{V_o}{V_{in}} = \frac{D}{1-D} = \frac{D}{D\prime} \tag{4.34}$$

$$\frac{I_o}{I_{in}} = \frac{D'}{D} \tag{4.35}$$

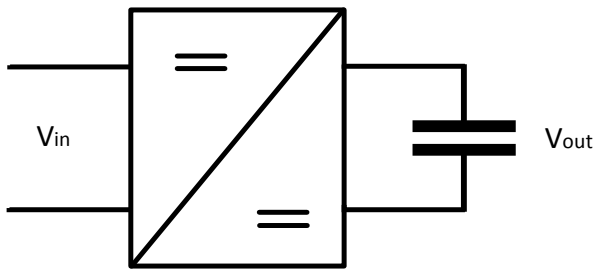

Figure 4.4. *Buck-boost converter with a capacitor at load*

In above simple buck-boost converter diagram V_{in} is the input voltage to the converter. In this ideal buck-boost converter model, the Ohmic and switching losses are modeled as series and parallel resistances respectively and Figure 4.4 can be redrawn as Figure 4.5

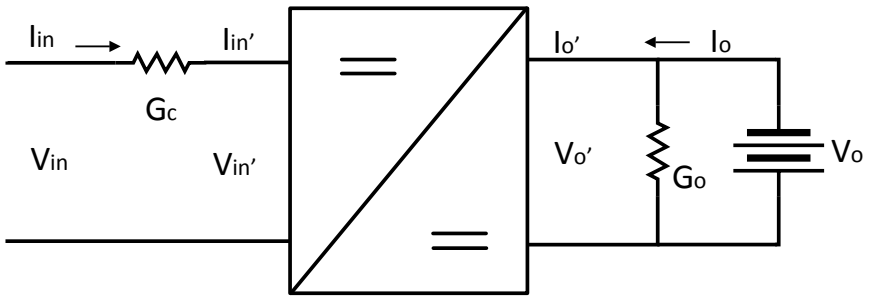

Figure 4.5. *Buck-boost converter configuration used in this research thesis.*

In steady state operation, a battery V_o can replace the capacitor, which draws no current [34].

From equations (4.34) and (4.35):

$$\frac{V_o}{V_{in}'} = \frac{D}{D'} \tag{4.36}$$

$$\frac{I_o'}{I_{in}'} = \frac{D'}{D} \tag{4.37}$$

From Figure 4.5:

$$I_{in}' = I_{in} = (V_{in} - V_{in}')G_c \tag{4.38}$$

$$I_{in}' = I_{in} = \left(V_{in} - V_o\left(\frac{D'}{D}\right)\right)G_c \tag{4.39}$$

$$I_{in}' = I_{in} = V_{in}G_c - V_oG_c\left(\frac{D'}{D}\right) \tag{4.40}$$

Now:

$$I_o' = -I_0 + G_oV_o \tag{4.41}$$

Comparing equations (4.37) and (4.41):

$$-I_0 + G_oV_o = I_{in}\left(\frac{D'}{D}\right) \tag{4.42}$$

From equation (4.40):

$$-I_0 + G_o V_o = \left(V_{in} G_c - V_o G_c \left(\frac{D'}{D} \right) \right) \left(\frac{D'}{D} \right) \tag{4.43}$$

⇒

$$I_0 = G_o V_o - V_{in} G_c \left(\frac{D'}{D} \right) + V_o G_c \left(\frac{D'}{D} \right)^2 \tag{4.44}$$

From equations (4.40) and (4.44) building the admittance matrix:

$$\begin{pmatrix} I_{in} \\ I_o \end{pmatrix} = \begin{pmatrix} G_c & -G_c\left(D'/D\right) \\ -G_c\left(D'/D\right) & G_o + G_c\left(D'/D\right)^2 \end{pmatrix} \begin{pmatrix} V_{in} \\ V_o \end{pmatrix} \tag{4.45}$$

Utilizing equation (4.30):

$$\begin{pmatrix} P_{in} \\ P_o \end{pmatrix} = \begin{pmatrix} V_{in} & 0 \\ 0 & V_o \end{pmatrix} \left\{ \begin{pmatrix} G_c & -G_c\left(D'/D\right) \\ -G_c\left(D'/D\right) & G_o + G_c\left(D'/D\right)^2 \end{pmatrix} \begin{pmatrix} V_{in} \\ V_o \end{pmatrix} \right\} \tag{4.46}$$

From above-assumed complex powers, nodal active and reactive powers equations at sending and receiving node arrived:

$$P_{in} = G_c V_{in}^2 - \left(D'/D\right) V_{\text{in}} V_{\text{o}} \left[G_c \cos(\theta_{\text{in}} - \theta_{\text{o}}) + B_{\text{dc}} \sin(\theta_{in} - \theta_{\text{o}}) \right]$$

$$P_o = \left(\left(D'/D\right)^2 G_c + G_o \right) V_o^2 - \left(D'/D\right)^2 V_{\text{in}} V_{\text{o}} \left[G_c \cos(\theta_{\text{o}} - \theta_{\text{in}}) + B_{\text{dc}} \sin(\theta_{\text{o}} - \theta_{\text{in}}) \right] \tag{4.47}$$

Due to the DC circuit, the susceptance and phase angles are zero so there will be zero reactive power contribution at both ends.

$$P_{in} = V_{in}^{\ 2} G_c - G_c\left(D'/D\right) V_{in} V_o \tag{4.48}$$

$$P_o = V_o^{\ 2} \left(G_o + G_c\left(D'/D\right)^2 \right) - G_c\left(D'/D\right) V_o V_{in} \tag{4.49}$$

By keeping the value of V_o a constant, the linearized system of equation for the above model of the DC-DC converter is shown in equation (4.50).

$$\begin{bmatrix} \Delta P_o \\ \Delta P_{in} \\ \Delta P_{in-o} \end{bmatrix}^r = \begin{bmatrix} 0 & 0 & \left(\partial P_{dc} / \partial\left(D'/D\right)\right) \\ 0 & 1 & \left(\partial P_{pv} / \partial\left(D'/D\right)\right) \\ \left(\partial P_{in-o} / \partial V_{dc}\right) V_o & \left(\partial P_{in-o} / \partial V_{pv}\right) V_{in} & \left(\partial P_{in-o} / \partial\left(D'/D\right)\right) \end{bmatrix}^r \times \begin{bmatrix} \Delta V_o / V_o \\ \Delta V_{in} / V_{in} \\ \Delta\left(D'/D\right) \end{bmatrix}^r \tag{4.50}$$

The mismatch power terms are given below:

$$\Delta P_{in} = P_{in}^{\ net} - P_{in}^{\ calc} \ ; \ \Delta P_o = P_o^{\ net} - P_o^{\ calc} ; \ \Delta P_{in-o} = P_{in-o}^{\ \ reg} - P_{in-o}^{\ \ calc}$$

State variable and updates are represented below:

$$\Delta\left(D^{'}/D\right)^{r} = \left(D^{'}/D\right)^{(r)} - \left(D^{'}/D\right)^{(r-1)}$$

4.7 Linearized system of equations

The equation (4.51) represents the linearized set of equations, using equations (4.33) and (4.50), comprising the double stage grid connected solar generator.

$$\begin{bmatrix} \Delta P_{vR} \\ \Delta Q_{vR} \\ \Delta P_o + \Delta P_{dc} \\ \Delta Q_o \\ \Delta Q_{o-vR} \\ \Delta P_{pv} \\ \Delta P_{pv-dc} \end{bmatrix}$$

$$= \begin{bmatrix} \partial P_{vR}/\partial\theta_{vR} & (\partial P_{vR}/\partial m_a)ma & 0 & (\partial P_{vR}/\partial\varphi) & \partial P_{vR}/\partial B_{eq} & 0 & 0 \\ \partial Q_{vR}/\partial\theta_{vR} & (\partial Q_{vR}/\partial m_a)ma & 0 & (\partial Q_{vR}/\partial\varphi) & \partial Q_{vR}/\partial B_{eq} & 0 & 0 \\ \partial P_o/\partial\theta_{vR} & (\partial P_o/\partial m_a)ma & 0 & (\partial P_o/\partial\varphi) & \partial P_o/\partial B_{eq} & 0 & \partial P_{dc}/\partial\left(D^{'}/D\right) \\ 0 & 0 & 1 & 0 & 0 & 0 & 0 \\ \partial Q_{o-vR}/\partial\theta_{vR} & (\partial Q_{o-vR}/\partial m_a)ma & 0 & (\partial Q_{o-vR}/\partial\varphi) & \partial Q_{o-vR}/\partial B_{eq} & 0 & 0 \\ 0 & 0 & 0 & 0 & 0 & 1 & \partial P_{pv}/\partial\left(D^{'}/D\right) \\ 0 & 0 & \left(\partial P_{pv-dc}/\partial V_{dc}\right)V_{dc} & 0 & 0 & \left(\partial P_{pv-o}/\partial V_{pv}\right)V_{pv} & \partial P_{pv-o}/\partial\left(D^{'}/D\right) \end{bmatrix}$$

$$\times \begin{bmatrix} \Delta\theta_{vR} \\ \Delta m_a/m_a \\ \Delta V_o/V_o \\ \Delta\varphi \\ \Delta B_{eq} \\ \Delta V_{pv}/V_{pv} \\ \Delta\left(D^{'}/D\right) \end{bmatrix} \qquad (4.51)$$

4.8 Implementation of the DC/DC converter power flow model

In order to implement the DC/DC converter in power flow model, it is taken as Load Tap Changing (LTC) transformer [26] so equations (4.48) and (4.49) becomes:

$$P_{in} = V_{in}{}^2 G_c - T_c G_c V_{in} V_o \tag{4.52}$$

$$P_o = -G_c T_c V_o V_{in} + V_o{}^2 \left(G_o + G_c T_c{}^2\right) \tag{4.53}$$

So, linearized system of equation becomes;

$$\begin{bmatrix} \Delta P_{in} \\ \Delta P_o \end{bmatrix} = -\begin{bmatrix} \partial \Delta P_{in} / \Delta V_{in} \partial & \partial \Delta P_{in} / \partial \Delta T_c \\ \partial \Delta P_o / \Delta V_{in} \partial & \partial \Delta P_o / \partial \Delta T_c \end{bmatrix} \times \begin{bmatrix} \Delta V_{in} \\ \Delta T_c \end{bmatrix} \tag{4.54}$$

$$P_o^{cal} = -G_c T_c V_o V_{in} + V_o{}^2 \left(G_o + G_c T_c{}^2\right) \tag{4.55}$$

As we are interested in power injected by the PVG so mismatch power term is given below:

$$\Delta P_o = \left(P_o^{gen} - P_o^{load}\right)^{Specified} - P_o^{cal} \tag{4.56}$$

The partial derivative for the term involved in output power calculation is given below:

$$\partial P_o / \partial T_c = -\left(-G_c V_o V_{in} + 2 T_c G_c V_o^2\right) \tag{4.57}$$

From above equations, we can calculate the ΔT_c

$$\Delta P_o = -\left(\frac{\partial P_o}{\partial T_c}\right) \Delta T_c \Rightarrow \Delta T_c = -\frac{\Delta P_o}{\left(\frac{\partial P_o}{\partial T_c}\right)} \tag{4.58}$$

The state variable updates are given below:

$$T_c^{k+1} = T_c^k + \Delta T_c \tag{4.59}$$

The equation describing the relationship between sending and receiving end of an LTC transformer can be obtained from [26]:

$$V_{in} = T_c V_o \tag{4.60}$$

From equation (4.34)

$$V_{in} = V_o \left(\frac{1-D}{D}\right) \tag{4.61}$$

$$T_c = \left(\frac{1-D}{D}\right) \Rightarrow D = \frac{1}{1+T_c} \tag{4.62}$$

The NR method takes 4 iterations to give the numerical results which are shown in Figure 4.6, for voltages at nodes *o* and *in* kept at 1 p.u. The staring value of Tc is 1. The power input from the PV panel is 1 p.u. the node *in* is taken to be the slack node.

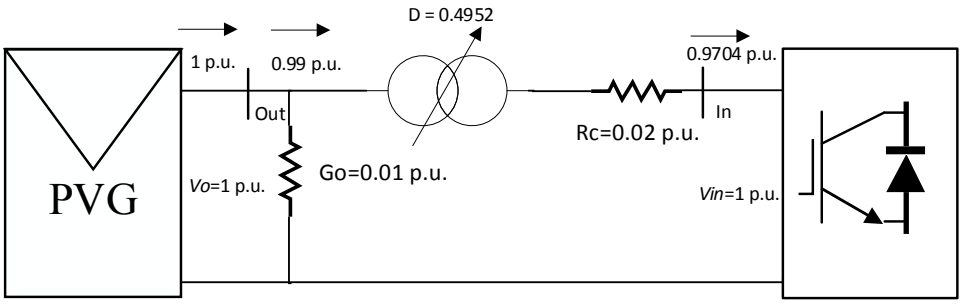

Figure 4.6. *DC-DC power flow.*

As from the results, we can see that total active power being injected at the *dc* end of the VSC is $P = 0.9704$ p.u. and the duty cycle at which the buck-boost converter is operating is $D = 0.4952$. The converter losses are 3%. Notice that the conductance of G_0 has a value of 1% and series connected resistance is 2%.

4.9 Summary

This chapter provided a review of electric power flows. The study involved in this chapter gave us an understanding of electric power buses, nodal power equations and iterative solutions. An iterative solution is required to solve the power flows and in this research thesis, the Newton Raphson method is used because of its strong convergence characteristics and its ability to solve any size of the electric power network with ease.

The Newton-Raphson method applied to electric power flows studies involve deep understanding of nodal power equations, non-linear system of equations and its solution by iteration. A matrix consisting of the coefficients of the linearized set of equations called, Jacobian matrix, was also explained in detail. A flow diagram consisting of all the main steps of solving and analyzing any electric power flow by using the Newton Raphson method was constructed and presented in this chapter.

Moreover, the representation of power electronic equipment, i.e., the mathematical modeling of VSC, buck-boost converter, and its implementation in the power flow Newton-Raphson method were explained in detail.

5. SIMULATION RESULTS

5.1 Introduction

In order to assess the performance of a system, a simulation platform is needed which could replicate the physical environment and yields the results which are the same as in the real world. As far as this research thesis is concerned, the simulation tool is MATLAB programming. The Newton Raphson power flow algorithm is used in power flows to assess the conditions and results of an electric power network. The paramount goal of this research thesis is the power flow assessment of grid-connected PV generators.

5.2 Test case 1

The three-bus system is presented in Figure 5.1 consist of two generators, one transmission line, one dc/dc converter and one ac/dc VSC. In this case, the dc buses, 3 and PVG, are controlled at 2 p.u. The node 1 is taken as slack bus and controlled at the voltage magnitude of 1 p.u. The phase angle of bus 1 is the reference only for bus 2, since dc buses have no angle i.e. zero values in the modelling approach adopted in this thesis.

The parameter used in this test case are: transmission line resistance and reactance are 0.01 p.u. and 0.10 p.u. respectively. Its sending end is connected to bus 1 and its receiving end to bus 2. The VSC resistance and reactance are 0.002 p.u. and 0.01 p.u. respectively. The nominal values VSC of the shunt conductance and susceptance are 0.002 p.u. and 0.5 p.u. respectively. A load is connected to bus 2 which consumes 0.25 p.u. of active power and 0.25 p.u. of reactive power. The parameters of dc/dc converter are taken as in Figure 4.6. The PV generator is assumed to be generating 1 p.u. of DC power.

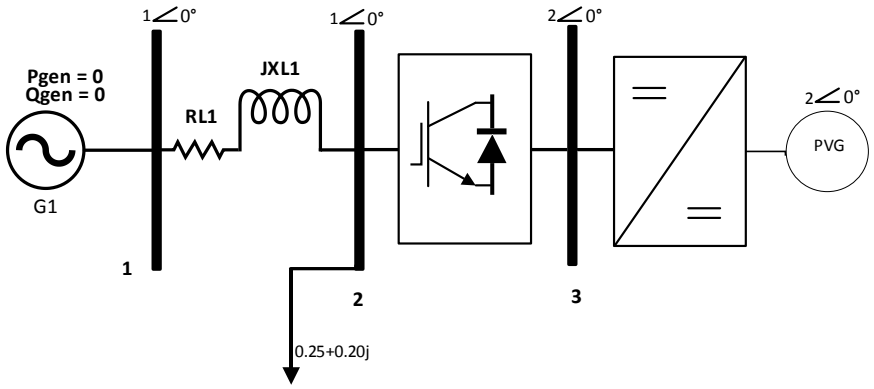

Figure 5.1. *Grid connected PVG*

5.2.1 No control mode

After taking away the switching and ohmic losses of the dc/dc converter, it injects 0.9554 p.u. of DC power at the dc bus of VSC. The dc/dc converter operates with duty cycle of $D = 0.4988$.

Three different test cases of VSC control are explained below, as mentioned in Table 4.2. The schematic diagram of the VSC is enclosed by the broken-line square. The Newton-Raphson method takes 6 iterations to yield the solution, as presented in Figure 5.2. In this mode of operation there is no control on VSC operation and therefore, the amplitude modulation of VSC takes the value of $m_a = 1$, with the phase shifter angle $\emptyset = 0°$. The equivalent susceptance takes the value of $B_{eq} = 0.5$ as initially declared, which produces 0.75 p.u. of reactive power. Due to the fact that there is no control on the VSC, 1.8671 p.u. of reactive power is injected into the receiving end of the VSC. Hence, the total reactive power supplied by the VSC into the transmission line is 2.5655 p.u. which consumes 0.0516 p.u. of reactive power. As PVG injects 0.9554 p.u. of active power and the VSC incurs losses of 0.0183 p.u. of active power and supplies 0.9371 p.u. of active power into the transmission line. As the load is connected to bus 2, 0.6451 p.u. of active and 1.9454 p.u. of reactive power arrive at bus 1, since the transmission line loss is 0.042 p.u. of active and 0.420 p.u. of reactive power. Notice that, as the voltage angle at the receiving end of the VSC in not zero, we cannot assume it to be a dc circuit. The losses are high in the case as there is no control on the VSC.

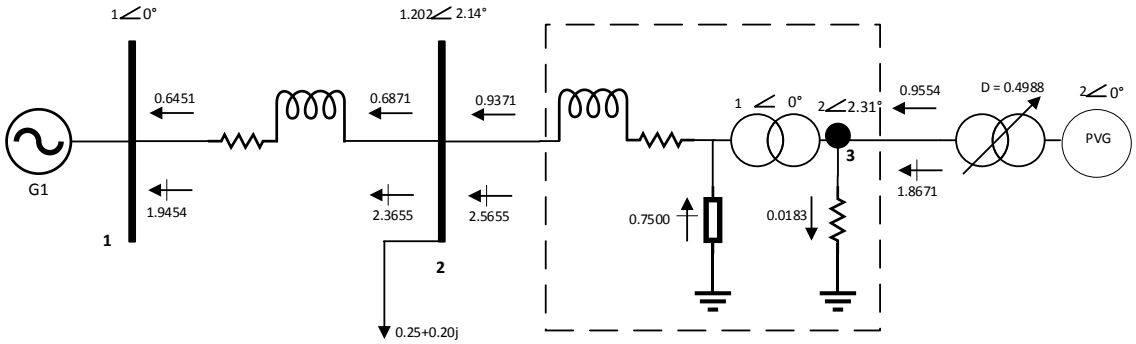

Figure 5.2. *No control.*

5.2.2 Voltage control mode

In this mode of operation, the VSC is tasked to control the voltage at its sending end which is connected to bus 2. So, the NR method produces the results after 6 iterations which are presented in Figure 5.3. Now the voltage at bus 2 is controlled at $VM = 1.05$

and its angle takes the value of $VA = 3.53°$. The amplitude modulation of VSC is $m_a = 0.8641$ with the phase shifter angle $\emptyset = 0°$. As phase shifter is not active, so 0.1278 p.u. of reactive power is injected into the receiving end of the VSC. The equivalent susceptance takes the value of $B_{eq} = 0.5$, as initially declared, which produces 0.56 p.u. of reactive power. As 0.1278 p.u. of reactive power is injected into the receiving end of the VSC, the total reactive power supplied by the VSC into the system is 0.6755 p.u. while consuming 0.0123 p.u. of reactive power. The VSC consumes 0.0104 p.u. of active power and delivers 0.9449 p.u. into bus 2, where the load point is connected. The transmission line losses are 0.0064 p.u. of active and 0.0643 p.u. of reactive power respectively. The power is injected into bus 1 is 0.6885 p.u. of active and 0.4112 of reactive power respectively. As we can see, by controlling the voltage, the losses have been reduced.

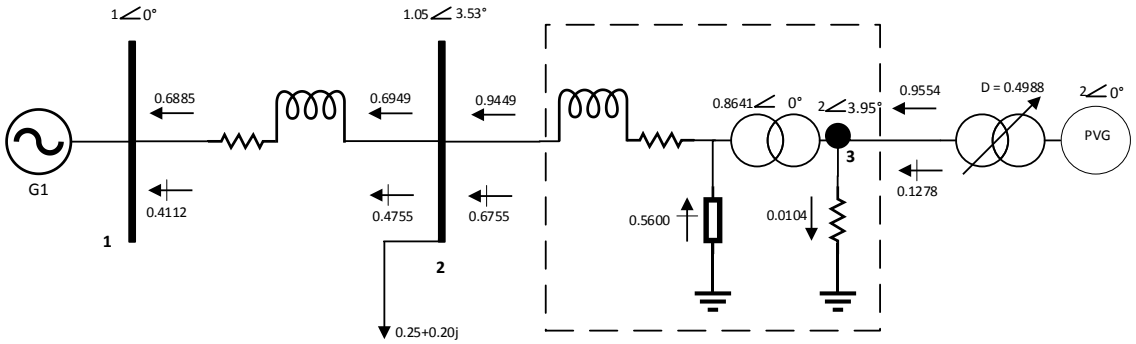

Figure 5.3. *Voltage control at the VSC's sending end.*

5.2.3 Full control mode

As discussed above, when using no power control and no voltage control, the dc circuit of the VSC produces reactive power and its nodal voltage has a phase angle, physically these conditions do not correspond to the characteristics of a dc bus. It can only be called a dc bus when there is no reactive power and the phase angle is zero i.e., no phase angle. In order to implement the full two stage converter topology for the PVG, the input and the output voltage of the dc converter should have zero phase angle. So, the model chosen to represent the VSC will fulfil these conditions when the VSC is operated with power control mode. Practically, the power can only be controlled at the dc bus, since power control on the AC bus of the VSC would not take account of the power losses. In this controlled operation mode of the VSC, the Newton-Raphson method takes 7 iterations to converge, the results are presented in Figure 5.4.

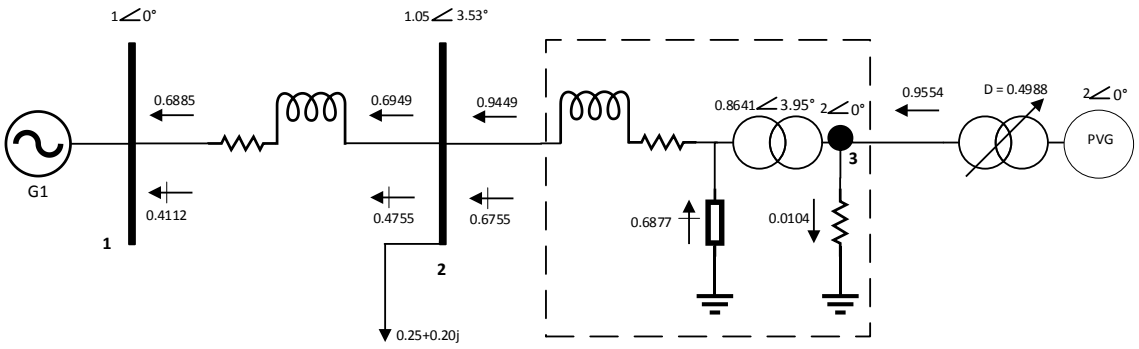

Figure 5.4. *Voltage control at sending and power control at receiving bus.*

The amplitude modulation of the VSC takes the value of $m_a = 0.8641$ with the phase shifter angle $\emptyset = 3.95°$. The equivalent susceptance takes the value of $B_{eq} = 0.6141$ which produces 0.6877p.u. of reactive power. The VSC consumes 0.0104 p.u. of active power and 0.0122 p.u. of reactive power to account for its switching and ohmic losses respectively, while supplying 0.6755 p.u. of reactive power into the AC system to control the voltage magnitude of bus 2 at $VM = 1.05$ and its angle takes the value of $VA = 3.53°$. The transmission line consumes 0.0064 p.u. of active power and 0.0643 p.u. of reactive power and bus 1 absorbs 0.6885 p.u. of active power and 0.4112 p.u. of reactive power respectively. As from these results, it is evident that the phase angle at the receiving end of the VSC is zero and losses are significantly decreased as compared to the case with *no control* mode. It is clear from the results presented in Figure 5.4 that the zero phase angles and the absence of the reactive power in the dc side of the VSC fulfil the necessary condition for the VSC to have an AC and a DC circuit.

5.3 Test Case 2: Micro-grid

The test case to conclude this master research thesis consists of a German Medium Voltage (MV) rural distribution network as presented in Figure 5.5 [35]. The original network has 12 nodes, 12 transmission lines and one 110/20 kV transformer. There are domestic and industrial loads connected to each node, except node 3.

The original network is modified to include the DG units and, as expected, the complexity level of the network increases, as presented in Figure 5.6. DG units are connected to every node except nodes1, 2 and 3. Node 1 is taken to be the slack bus in this network. The modified MV network consists of 39 nodes, 16 generators, 15 transformers, 13 VSCs and 8 buck-boost converters. There are 8 PVGs connected to their respective nodes using the two-stage converter and a step-up transformer. Every other DG unit is connected to the network via a VSC and transformer. The base voltage chosen for this test case is $S_{base} = 10\ MVA$ and the original values were converted into the per unit system. As rated voltage for this network is 20 kV so the base impedance can be calculated from the equation (5.1).

$$Z_{base} = \frac{V_{ref}^2}{S_{base}} \tag{5.1}$$

$$\Rightarrow Z_{base} = 40\Omega$$

5.3.1 Modeling of distributed energy resources

The modified network contains different distributed energy resources such as, photovoltaic, battery, fuel cell, wind turbine and Combined Heating and Power (CHP) diesel. So they are modelled into power flow program differently. The modeling of PV is explained in this research thesis. The battery bank is modeled as negative load connected to dc bus of the VSC when injecting the power into the VSC and as a positive load point when it is charging i.e. consuming the power. The fuel cell is always modeled as negative load connected to the dc bus of the VSC. The CHP diesel is modeled as synchronous generator. The wind turbine is assumed to operate with 0.9 lagging power factor, so 1500 kW wind turbine consumes 750kVAR of reactive power. It is modeled as negative active power load and positive reactive power load respectively.

The relevant date of the loads, transmission lines, transformers, DG units, dc/dc and dc/ac converters is given in Appendix A1, A2, A3, A4 A5 and A6, respectively.

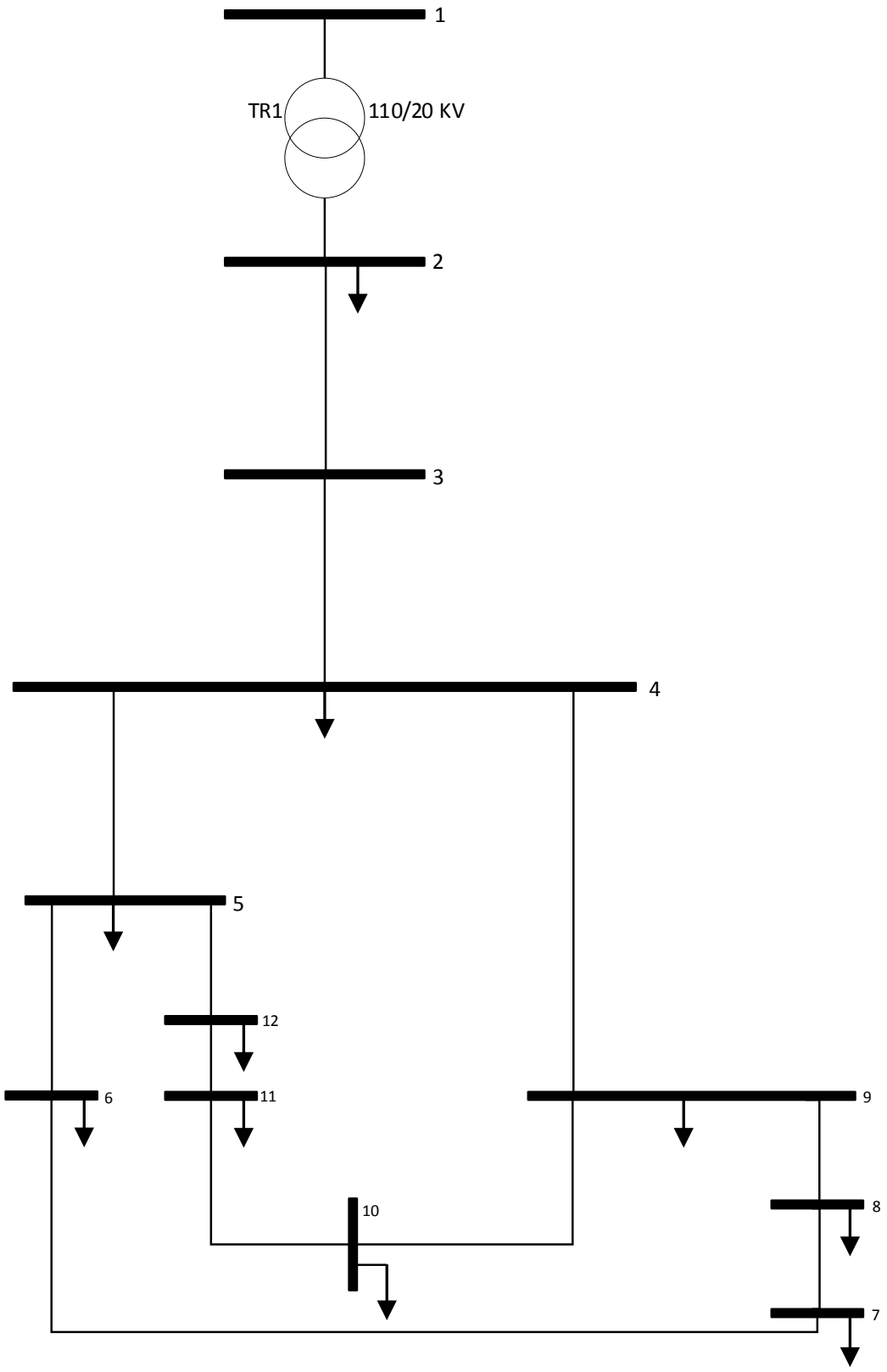

Figure 5.5. *Medium-Voltage network.*

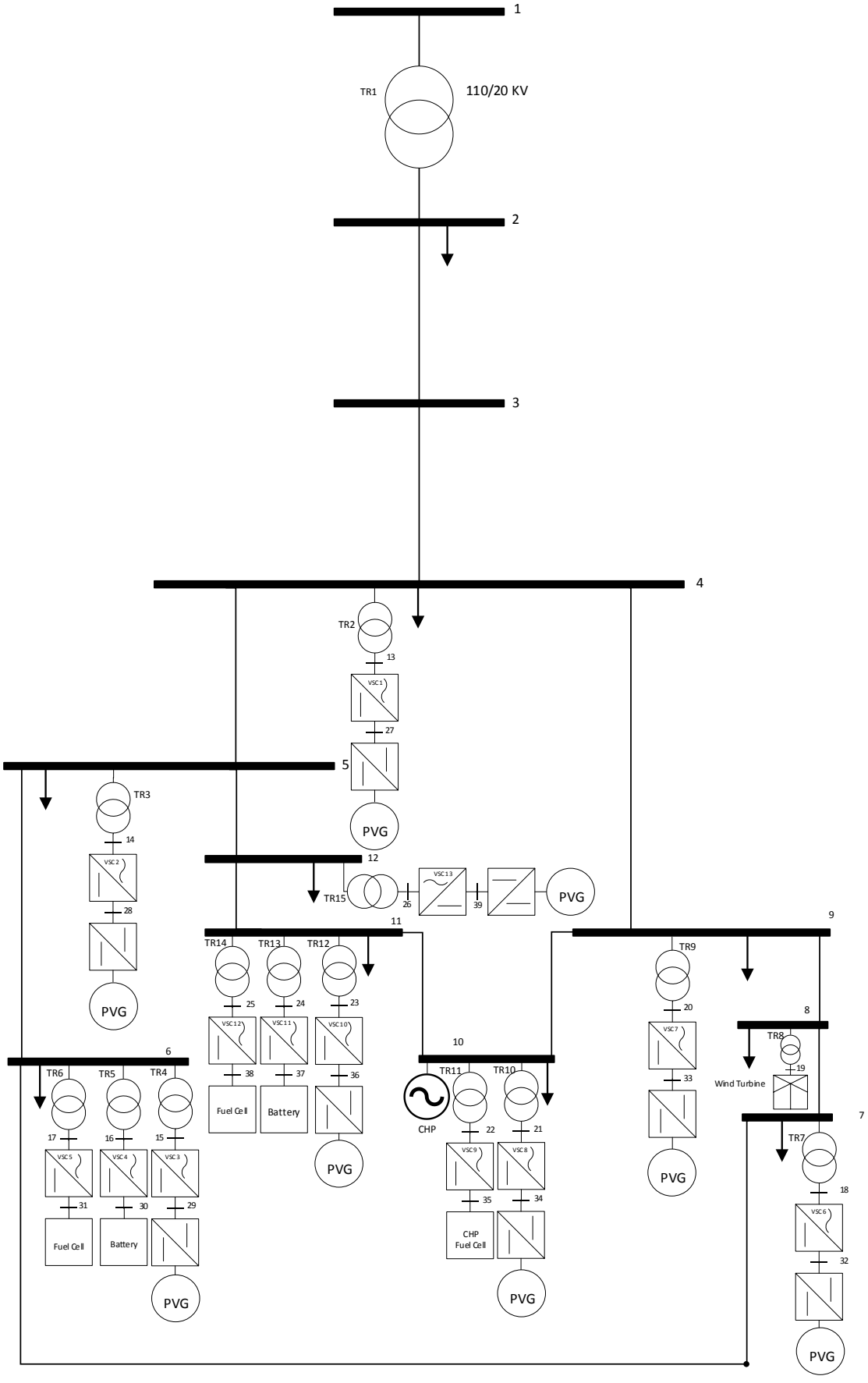

Figure 5.6. *Micro-grid test case.*

In this micro-grid test case, the dc node between the two converters of a PV system is taken as a slack bus and all VSCs are operating in voltage and power control mode. The dc buses, from 27 to 39, are controlled at 2 p.u. The results of the PVGs and dc/dc converters are given below:

Table 5.1. *PVGs and dc/dc converter results.*

Generated power (p.u.)	**Duty cycle**	**Injected power (p.u.)**	**Power Loss (p.u.)**
0.002	0.5	0.00190	0.0001
0.002	0.5	0.00190	0.0001
0.003	0.5	0.00290	0.0001
0.003	0.5	0.00290	0.0001
0.003	0.5	0.00290	0.0001
0.003	0.5	0.00290	0.0001
0.004	0.5	0.00380	0.0002
0.001	0.5	0.00096	0.00004

All the dc converters are operating at the duty cycle of $D = 0.5$. As described in section 4.8, the series resistance and conductance of the dc converters is 2 and 1 percent of the input power respectively. The series resistance and shunt conductance of each converter takes the value according to the input power. This data is also presented in Appendix A5. The active power being injected into the VSC is presented in the third column of Table 5.1. The power losses are referred as switching losses and ohmic losses respectively.

In the next part of the micro-grid test case, the Newton Raphson method converges in 8 iterations and results are shown in the figures and tables below.

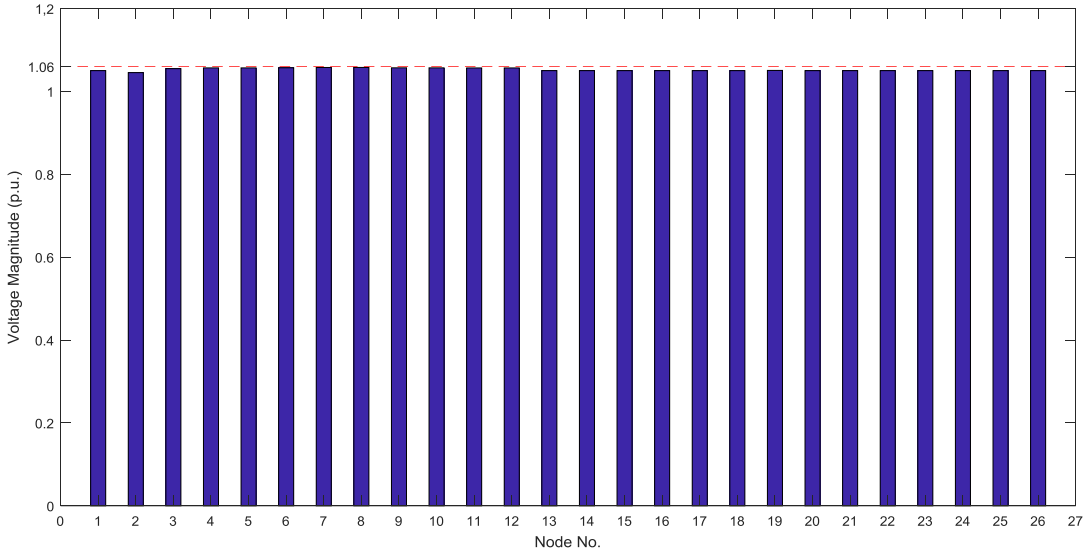

Figure 5.7. *AC nodes voltage magnitudes.*

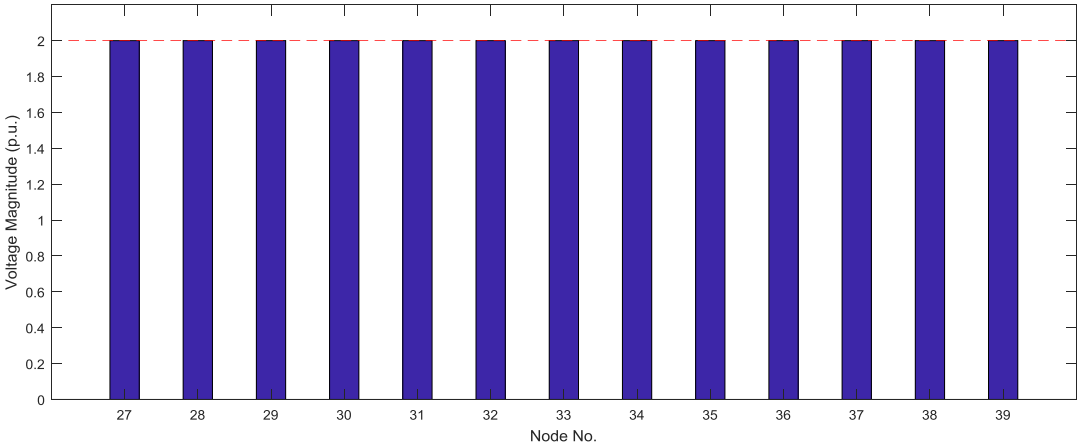

Figure 5.8. *DC buses voltage magnitudes.*

In Figure 5.7, the nodes 1-12 which comprise the original MV network the voltage profile improvement is very significant as compared to the results shown in [35], before the inclusion of DG units. The voltage magnitude level of these nodes is well within the limits of $100 \pm 6\%$. The nodes from 13-26 connected with the sending ends of the VSCs, which are operating in full control mode, take the voltage magnitude value of $VA = 1.05$. Figure 5.8 presents the dc buses of the VSCs which are being controlled at 2 p.u. Figure 5.9 presents the phase angles of the AC nodes only as all the DC nodes of the micro-grid test case have zero phase angle.

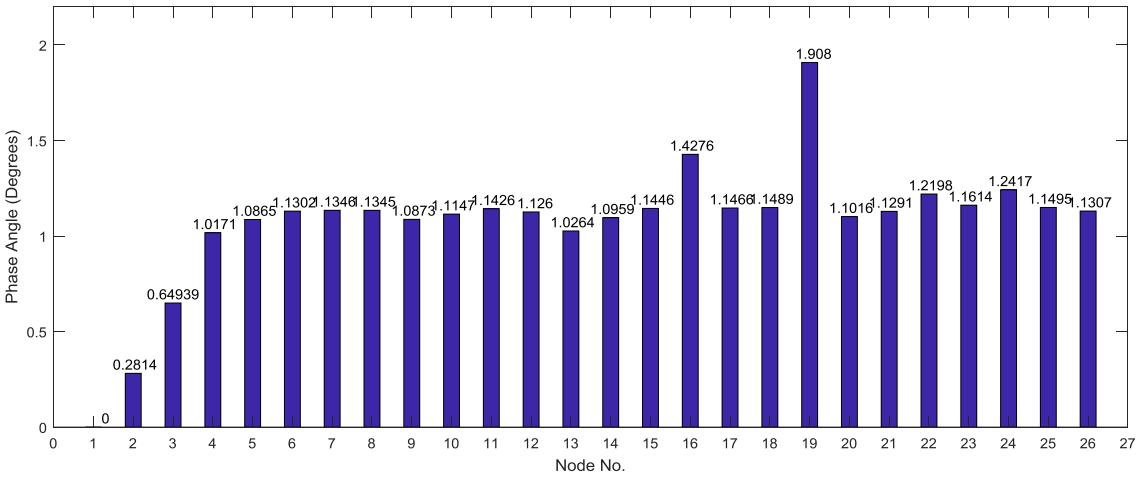

Figure 5.9. *Phase angles of AC nodes.*

As in this micro-grid test case, all the VSCs are operating in full control mode so the relevant results are shown in the tables below.

Table 5.2. *VSCs results.*

VSC No.	$(\boldsymbol{m_a})$	**(∅)**	$(\boldsymbol{B_{eq}})$
1	0.8568	1.0310	-0.0632
2	0.8568	1.1005	-0.0633
3	0.8568	1.1498	-0.0661
4	0.8568	1.4613	-0.0659
5	0.8568	1.1520	-0.0661
6	0.8567	1.1545	-0.0727
7	0.8568	1.1068	-0.0648
8	0.8568	1.1342	-0.0642
9	0.8568	1.2341	-0.0641
10	0.8568	1.1669	-0.0620
11	0.8568	1.2553	-0.0620

12	0.8568	1.1538	-0.0620
13	0.8568	1.1348	-0.0623

Table 5.3. *VSCs active and reactive powers.*

VSC No.	Ac bus	Dc bus	Power losses of the VSCs
1	-0.0018 + 0.0697j	0.0019 - 0.0000i	0.0001 + 0.0696j
2	-0.0018 + 0.0697j	0.0019 - 0.0000i	0.0001 + 0.0697j
3	-0.0028 + 0.0728j	0.0029 - 0.0000i	0.0001 + 0.0727j
4	-0.0576 + 0.0726j	0.0600 - 0.0000i	0.0024 + 0.0725j
5	-0.0032 + 0.0728j	0.0033 - 0.0000i	0.0001 + 0.0727j
6	-0.0028 + 0.0801j	0.0029 - 0.0000i	0.0001 + 0.0800j
7	-0.0028 + 0.0714j	0.0029 - 0.0000i	0.0001 + 0.0713j
8	-0.0028 + 0.0704j	0.0029 - 0.0000i	0.0001 + 0.0706j
9	-0.0203 + 0.0707j	0.0212 - 0.0000i	0.0009 + 0.0706j
10	-0.0036 + 0.0683j	0.0038 - 0.0000i	0.0002 + 0.0683j
11	-0.0192 + 0.0683j	0.0200 - 0.0000i	0.0008 + 0.0683j
12	-0.0013 + 0.0683j	0.0014 - 0.0000i	0.0001 + 0.0683j
13	-0.00091 + 0.0687j	0.00096 - 0.0000i	0.00004 + 0.0686j

It can be seen from these results that all the VSCs are injecting the active power generated by the DG units. The VSCs should be designed in such a way that they inject the active power into the system. The shunt conductance of each VSC consumes 1% of the power input from the dc/dc converters. So every VSC has the different value of the shunt conductance, in order to make the active power go through the VSC into the network. This data is provided in Appendix A6.

The transmission lines powers at sending, receiving end and their losses are given below:

Table 5.4. *Transmission lines active and reactive powers.*

Transmission line	Sending end	Receiving end	Losses
1	-0.2539 + 0.0093j	0.2563 - 0.0140j	0.0024 - 0.0046j
2	-0.2563 + 0.0140j	0.2582 - 0.4217j	0.0018 - 0.4078j
3	-0.1279 + 0.2532j	0.1282 - 0.3086j	0.0003 - 0.0553j
4	-0.1083 + 0.1134j	0.1084 - 0.1492j	0.0001 - 0.0358j
5	-0.0521 - 0.0726j	0.0522 - 0.0461j	0.0000 - 0.1187j
6	-0.0544 - 0.0359j	0.0544 + 0.0233j	0.0000 - 0.0126j
7	0.0949 - 0.1013j	0.0947 - 0.0300j	0.0001 - 0.1313j
8	-0.0420 + 0.1727j	0.0421 - 0.1924j	0.0001 - 0.0196j
9	0.0063 + 0.0465j	-0.0062 - 0.0988j	0.0000 - 0.0522j
10	0.0250 - 0.1091j	-0.0249 + 0.0880j	0.0000 - 0.0211j
11	0.0225 - 0.1580j	-0.0224 + 0.1239j	0.0001 - 0.0340j
12	-0.1335 + 0.0963j	0.1337 - 0.2161j	0.0002 - 0.1198j

The transmission lines losses are calculated by the difference of powers at sending and receiving ends so if we see transmission lines 5 and 6 have very low losses due to the fact that large DG units are connected at these nodes. This is also explained in Figure 5.10.

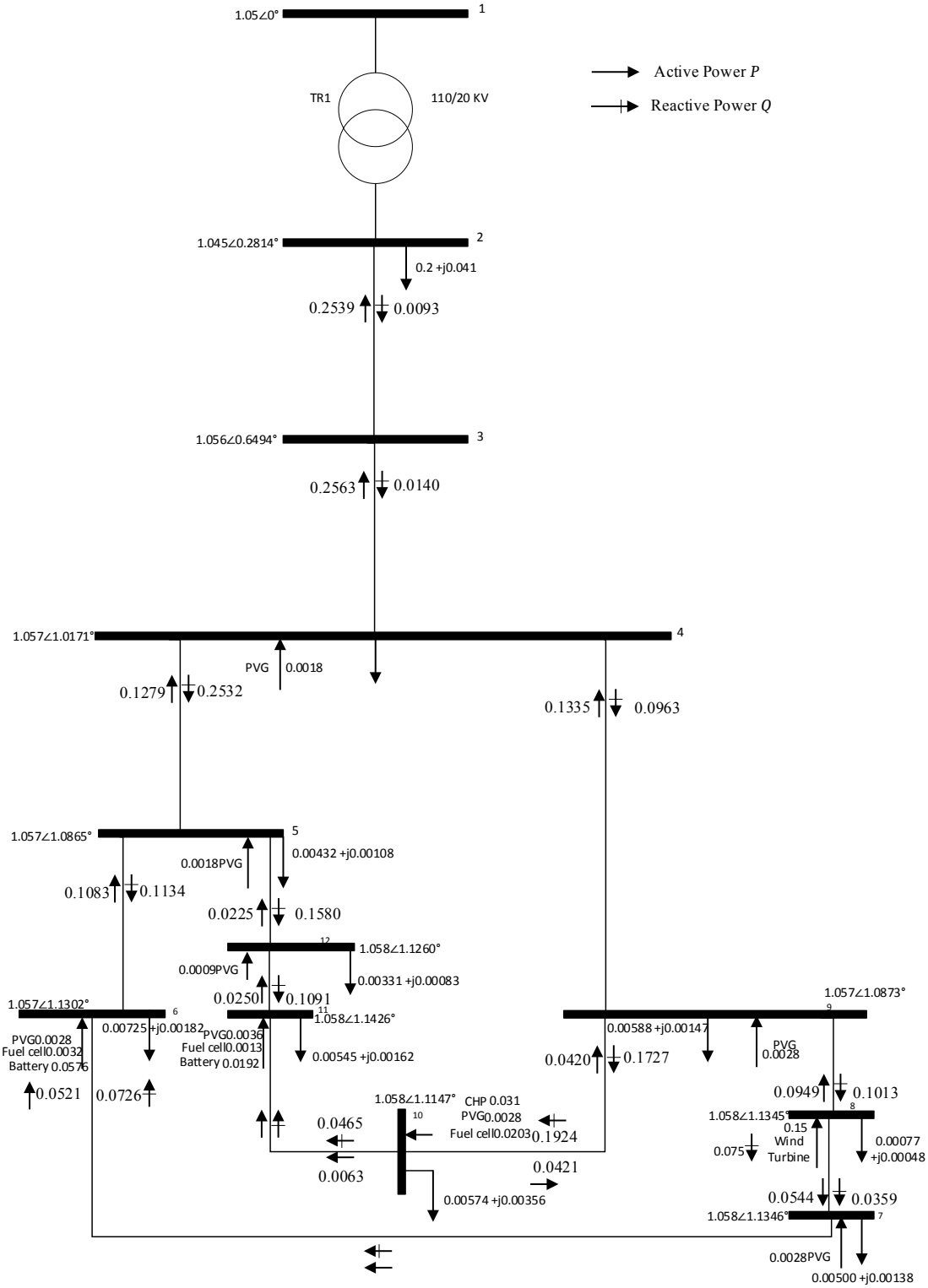

Figure 5.10. *Transmission lines active and reactive power directions with values at their sending ends and power injections at the nodes with voltage magnitude and phase angle.*

As the electric power into the network is being supplied through a 110kV transformer and every DG unit is connected to the network via a transformer so the results of active and reactive powers are given below.

Table 5.5. *Transformers active and reactive powers.*

Transformer No.	Sending end	Receiving end
1	-0.0539 + 0.0508j	0.0539 - 0.0503j
2	-0.0018 + 0.0701j	0.0018 - 0.0697j
3	-0.0018 + 0.0702j	0.0018 - 0.0697j
4	-0.0028 + 0.0733j	0.0028 - 0.0728j
5	-0.0576 + 0.0734j	0.0576 - 0.0726j
6	-0.0032 + 0.0733j	0.0032 - 0.0728j
7	-0.0028 + 0.0807j	0.0028 - 0.0801j
8	-0.1500 + 0.0775j	0.1500 - 0.0750j
9	-0.0028 + 0.0718j	0.0028 - 0.0714j
10	-0.0028 + 0.0711j	0.0028 - 0.0707j
11	-0.0203 + 0.0712j	0.0203 - 0.0707j
12	-0.0036 + 0.0688j	0.0036 - 0.0683j
13	-0.0192 + 0.0688j	0.0192 - 0.0683j
14	-0.0013 + 0.0688j	0.0013 - 0.0683j
15	-0.0009 + 0.0691j	0.0009 - 0.0687j

The active and reactive power flows in this test case involving transformers, VSCs, dc/dc converters and DG units are represented in Figure 5.11 and Figure 5.12.

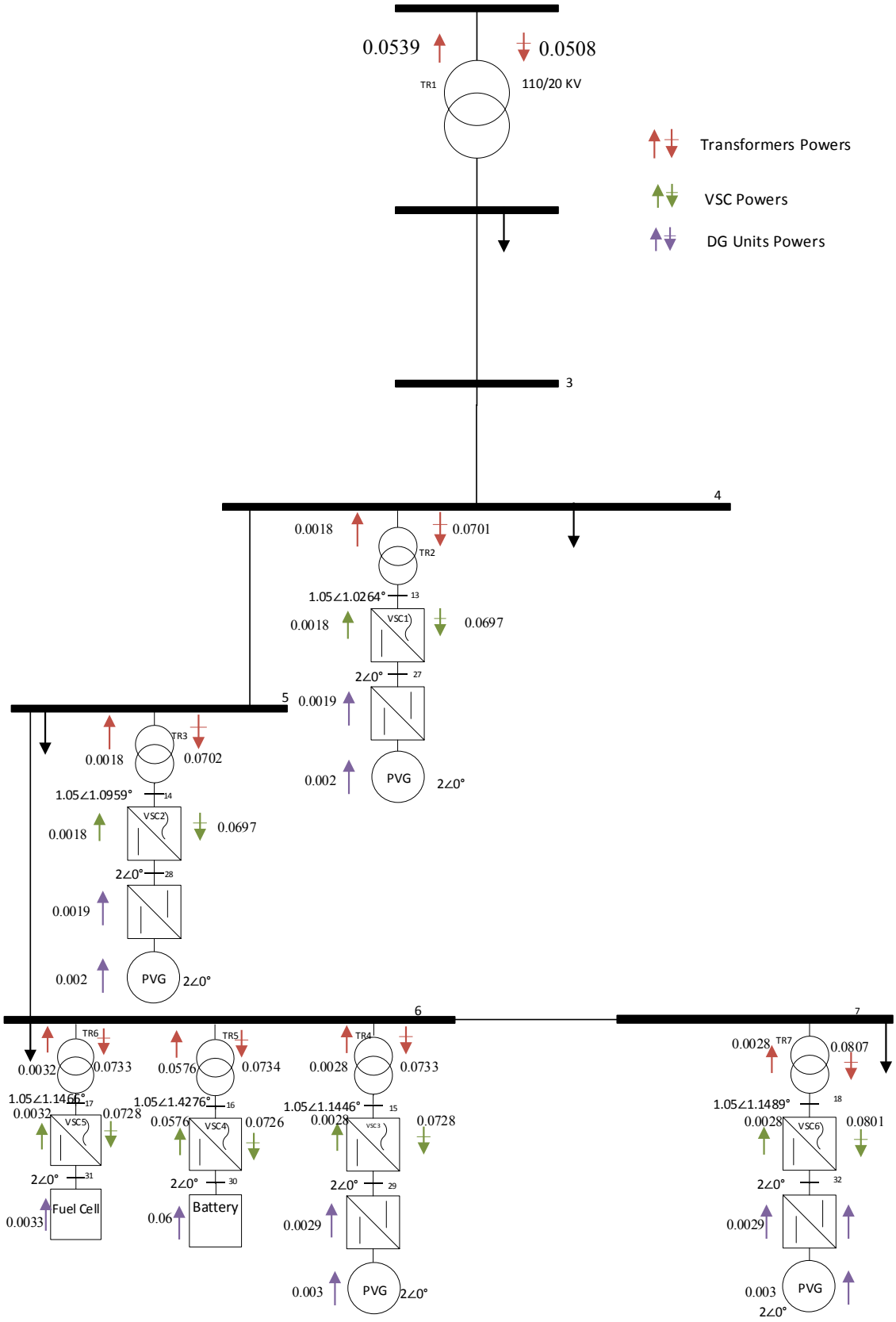

Figure 5.11. *Micro-Grid active and reactive power directions and values connected to the nodes 1-7 with voltage magnitude and phase angle.*

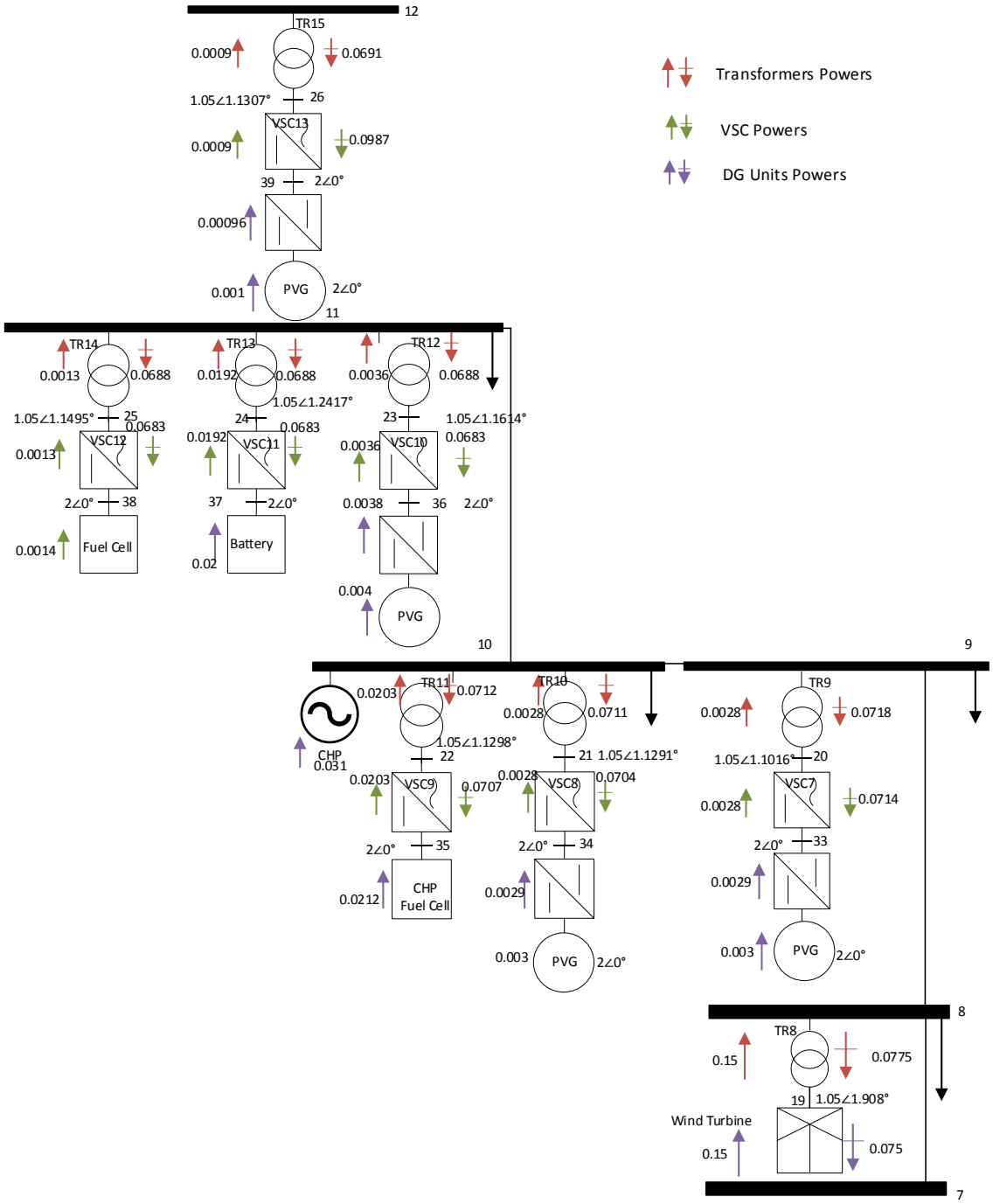

Figure 5.12. *Micro-Grid active and reactive power directions and values connected to the nodes 7-12 with voltage magnitude and phase angle.*

5.4 Summary

In this chapter, the inclusion of a PVG model in electric power flows, using a two-stage converter topology, has been carried out. An illustration of the three different control modes of the VSC was also presented. The results show that the VSC should be operated in full control mode in order to make the dc-dc and dc-ac converter topology model to work for grid connected PVG applications. Later on, this approach was applied in a micro grid DG scenario where a German MV distribution network was selected, redesigned and presented in this chapter. The results show that the voltage profile was improved significantly and that the DG units supplied active power to the nodes whereas, reactive power was absorbed by the VSCs.

6. CONCLUSIONS AND FUTURE WORK

6.1 General conclusions

The future of smart grids depends heavily on the integration of distribution generation based on the renewable energy resources. The global warming and expanding of the urban population demand continuous and uninterrupted electricity supply. In this ask the solar power generation has shown an impressive growth during the last few years. In these developments, the modern power electronic equipment is rapidly becoming the backbone of modern electric power networks.

In this master thesis research work, the integration of the photovoltaic generator model into the power flow application tool, using the Newton Raphson iterative method, was achieved. The computer program was written in MATLAB programming. The PV panels were assumed to be working at their maximum power outputs as given by their MPPT mechanism.

After doing some arduous algebra the combined set of linearized equations has been successfully constructed and presented which involves, PVG, dc-dc converter and VSC. In the next step the dc converter implementation is successfully carried out in the Newton Raphson method to integrate it with the VSC. At this point, this computer program is ready to increase the network size of electricity distribution network, involving grid connected PVG or any other renewable in two-stage converter topology.

6.2 Learning and issues

This research work has been the most challenging work for the author and during completion of this research, the author has developed the skills of MATLAB coding and learned the working operations of electric power flows. As the VSC is involved in constructing the STATCOM and HVDC links so this research thesis has been a learning milestone for the author.

Since the inclusion of dc/dc converter with the modern VSC was the paramount goal so first, the reduced admittance matrix approach was carried out but in that scenario, there was no control on the dc end of the VSC. Then combined admittance matrix approach was followed and the most challenging part was to put it in the MATLAB programming and therefore, dc/dc converter was lumped together with PVG to construct a proper two-stage converter topology.

6.3 Future work possibilities

This research work mainly focuses on positive sequence power flows under steady-state conditions but the inclusion of dc/dc converter opens a new way of investigating the dynamic response of this PVG approach i.e. combined linearized system of equations. Moreover, the approach to build the two-stage converter topology using two VSCs in tandem, need to be investigated. In this approach, the receiving ends of the VSCs do not have a common point like back-to-back HVDC [36] instead the dc end of the one VSC is connected to PVG and its sending end lumped with the dc end of the second VSC.

REFERENCES

[1] U. E. I. Administration, "Internation Energy Outlook 2016," 11 May 2016. [Online]. Available: http://www.eia.gov/outlooks/ieo/world.cfm.

[2] J. Balázs-Hegedűs, "Energy Sources," 2017. [Online]. Available: http://balazshegedus.com/energy-sources-isometric-icon-set/. [Accessed 31 August 2017].

[3] B. K. Bose, *Global Warming: Energy, Environmental Pollution, and the Impact of Power Electronics,* March 2010.

[4] "Solar energy will surpass nuclear by the end of the year," World Economic Forum, 5 September 2017. [Online]. Available: https://www.weforum.org/agenda/2017/09/solar-energy-will-surpass-nuclear-by-the-end-of-the-year?utm_content=buffer7d129&utm_medium=social&utm_source=twitter.com&utm_campaign=buffer. [Accessed September 2017].

[5] P. Pakonen, A. Hilden and T. Suntio, "Grid-connected PV power plant induced power quality problems — Experimental evidence," in *2016 18th European Conference on Power Electronics and Applications (EPE'16 ECCE Europe)*, 2016.

[6] R. Rapier, "A Record Year For Renewable Energy," Forbes, June 2016. [Online]. Available: https://www.forbes.com/sites/rrapier/2016/06/03/a-record-year-for-renewable-energy/#785f7f4e6c90. [Accessed 31 August 2017].

[7] A. Pazynyc, "A study of the harmonic content of distribution power grids with distributed PV systems," 13 August 2014. [Online]. Available: http://dspace.cc.tut.fi/dpub/handle/123456789/22309.

[8] R. Li, M. Armstrong and S. Gadoue, "On-line parameter estimation of non-minimum phase switch mode power DC-DC boost converters," in *8th IET International Conference on Power Electronics, Machines and Drives (PEMD 2016)*, 2016.

[9] H. Häberlin, Photovoltaics: System Design and Practice, John Wiley & Sons, Ltd, 2012.

[10] S. R. Wenham, M. A. Green, M. E. Watt and R. Corkish, Applied Photovoltaics, vol. II, Earthscan, 2007.

[11] S. Valkealahti, "Lecture Notes Solar Power Systems," Tampere University of Technology, 2016.

[12] S. Sumathi, L. Ashok Kumar and P. Surekha, Solar PV and Wind Energy Conversion Systems An Introduction to Theory, Modeling with MATLAB/SIMULINK, and the Role of Soft Computing Techniques, Springer International Publishing, 2015.

[13] D. Rekioua and E. Matagne, Optimization of Photovoltaic Power Systems Modelization, Simulation and Control, London: Springer-Verlag London Limited, 2012.

[14] T. Leroy, "Simple Solar Cell And Panel Model," 4 May 2011. [Online]. Available: https://se.mathworks.com/matlabcentral/fileexchange/31305-simple-solar-cell-and-panel-model?focused=5187488&tab=function. [Accessed August 2017].

[15] P. Breza, "Master Thesis: Modelling and simulation of a PV generator for applications on distributed generation systems," 15 November 2013. [Online]. Available: https://repository.tudelft.nl/islandora/object/uuid:259fa81e-fa57-48f3-802a-f209f1e74006/datastream/OBJ. [Accessed September 2017].

[16] R. Messenger and J. Ventre, Photovoltaic systems Engineering, CRC PRESS, 2003.

[17] S. Lacey, "Global Solar Capacity Set to Surpass Nuclear for the First Time," Greentech Media, 21 August 2017. [Online]. Available: https://www.greentechmedia.com/articles/read/global-solar-capacity-set-to-surpass-global-nuclear-capacity. [Accessed 11 September 2017].

[18] N. Mohan, T. M. Undeland and W. P. Robins, in *Power Electronics. Converters, Applications and Design*, John Wiley & Sons, Inc., 1995.

[19] T. Suntio, "Lecture Notes Steady State Analysis of Switched-Mode Power Supplies," 2010.

[20] J. M. Maza-Ortega, E. Acha, S. Gracia and A. Gomez-Exposito, "Overview of power electronics technology and applications in power generation transmission and distribution," *Modern Power Systems Clean Energy,* 2017.

[21] E. Acha, C. R. Fuerte-Esquivel, H. A.-P.´rez and C.´. Angeles-Camacho, FACTS: Modelling and Simulation in Power Networks, John Wiley & Sons Ltd., 2005.

[22] N. G. Hingorani and L. Gyugyi, Understanding FACTS: Concepts and Technology of Flexible AC Transmission Systems, IEEE, 2000.

[23] N. L. Diaz, F. H. Barbosa and C. L. Trujillo, " Implementation of Nonlinear power flow controllers to control a VSC," in *International Power Electronics and Motion Control Conference*, 2008.

[24] G. Radomski, "Modelling and Modulation of Voltage Source Converter," in *International Power Electronics and Motion Control Conference*, 2008.

[25] S. Sarkar, P. Vijayan, D. C. Aliprantis and V. Ajjarapu, "Effect of Grid Voltage Unbalance on Operation of a Bi-directional Converter," in *Power Symposium, 2008. NAPS '08. 40th North American*, 2008.

[26] E. Acha and B. Kazemtabrizi, "A New STATCOM Model for Power Flows Using the Newton–Raphson Method," *IEEE TRANSACTIONS ON POWER SYSTEMS,* vol. 28, no. 3, pp. 2455-2465, 2013.

[27] E. Acha, "Lecture Notes Flexible Transmission Systems," Tampere University of Technology, 2014.

[28] L. M. C. González, "Modelling of Multi-terminal VSC-HVDC Links for Power Flows and Dynamic Simulations of AC/DC Power Networks," 2016. [Online]. Available: https://tutcris.tut.fi/portal/files/8787926/gonzalez_1445.pdf. [Accessed 2017].

[29] B. Kazemtabrizi, "Mathematical modelling of multi-terminal VSC-HVDC links in power systems using optimal power flows," 2011. [Online]. Available: http://theses.gla.ac.uk/2937/.

[30] E. Acha, V. Agelidis, O. Anaya-Lara and T. Miller, Power Electronic Control in Electrical Systems, Elsevier Ltd., 2002.

[31] J. T. Betts, Practical Methods for Optimal Control Using Nonlinear Programming, Society for Industrial and Applied Mathematics, 2001.

[32] E. Acha, "Lecture Notes Electric Power Systems," Tampere University of Technology, 2016.

[33] C. Angeles-Camacho, O. Tortelli, E. Acha and C. Fuerte-Esquivel, "Inclusion of a high voltage DC-voltage source converter model in a Newton-Raphson power flow algorithm," *Generation, Transmission and Distribution, IEE Proceedings,* vol. 150, pp. 691-696, 2003.

[34] J. W. Nilsson and S. A. Riedel, ELECTRIC CIRCUITS, Upper Saddle River, New Jersey: Prentice Hall, 2011.

[35] K. Rudion, A. Orths, Z. A. Styczynski and K. Strunz, "Design of Benchmark of Medium Voltage Distribuition Network for Investigation of DG Integration," in *IEEE*.

[36] E. Acha, B. Kazemtabrizi and L. M. Castro, "A New VSC-HVDC Model for Power Flows Using the Newton-Raphson Method," *IEEE TRANSACTIONS ON POWER SYSTEMS,* vol. 28, no. 3, pp. 2602-2612, 2013.

APPENDIX A. MICRO GRID TEST CASE DATA

A1. Load Data

Load No.	Node No.	Load Type	P (p.u.)	Q(p.u.)
1	2	Domestic	0.15000	0.03100
2	2	Industry	0.05000	0.01000
3	4	Domestic	0.00276	0.00069
4	4	Industry	0.00224	0.00139
5	5	Domestic	0.00432	0.00108
6	6	Domestic	0.00725	0.00182
7	7	Domestic	0.00550	0.00138
8	8	Industry	0.00077	0.00048
9	9	Domestic	0.00588	0.00147
10	10	Industry	0.00574	0.00356
11	11	Industry	0.00068	0.00042
12	11	Domestic	0.00477	0.00120
13	12	Domestic	0.00331	0.00083

A2. Transmission Lines Data.

Line No.	Sending end	Receiving end	Length (*km*)	*Z = R+jX*	Capacitance *nF/km*
1	2	3	2.82	0.579+0.367j	158,88
2	3	4	4.42	0.164+0.113j	6608
3	4	5	0.61	0.164+0.113j	6480
4	5	6	0.56	0.354+0.129j	4560
5	6	7	1.54	0.336+0.126j	5488
6	7	8	0.24	0.256+0.13j	3760
7	8	9	1.67	0.294+0.123j	5600
8	9	10	0.32	0.339+0.13j	4368
9	10	11	0.77	0.399+0.133j	4832
10	11	12	0.33	0.367+0.133j	4560
11	12	5	0.49	0.423+0.134j	4960
12	4	9	1.3	0.172+0.115j	6576

Frequency used for each transmission line: $f = 50\ Hz$.

A3. Transformers Data.

Trans-former No	Sending end	Receiving end	Resistance (p.u.)	Reactance (p.u.)	Tap (p.u.)
1	1	2	0.00	0.10	1
2	4	13	0.00	0.10	1
3	5	14	0.00	0.10	1
4	6	15	0.00	0.10	1
5	6	16	0.00	0.10	1
6	6	17	0.00	0.10	1
7	7	18	0.00	0.10	1
8	8	19	0.00	0.10	1
9	9	20	0.00	0.10	1
10	10	21	0.00	0.10	1
11	10	22	0.00	0.10	1
12	11	23	0.00	0.10	1
13	11	24	0.00	0.10	1
14	11	25	0.00	0.10	1
15	12	26	0.00	0.10	1

A4. DG Data.

DG No.	Node No.	DG Type	P (kW)
1	27	Photovoltaic	20
2	28	Photovoltaic	20
3	29	Photovoltaic	30
4	30	Battery	600
5	31	Fuel cell	33
6	32	Photovoltaic	30
7	19	Wind Turbine	1500
8	33	Photovoltaic	30
9	34	Photovoltaic	30
10	35	Fuel cell	212
11	10	CHP Diesel	310
12	36	Photovoltaic	40
13	37	Battery	200
14	38	Fuel cell	14
15	39	Photovoltaic	10

A5. DC/DC Converters Data.

Converter No	Resistance (Ω)	Shunt conductance (S)	Initial Value of T_c (p.u.)
1	0.0016	0.0008	1
2	0.0016	0.0008	1
3	0.0024	0.0012	1
4	0.0024	0.0012	1
5	0.0024	0.0012	1
6	0.0024	0.0012	1
7	0.0032	0.0016	1
8	0.0008	0.0004	1

A6. VSCs Data.

VSC No.	Shunt conduct-ance (S)	Initial Values		
		m_a (p.u.)	B_{eq} (p.u.)	∅ (p.u.)
1	0.0008	1.0	0.5	0
2	0.0008	1.0	0.5	0
3	0.0012	1.0	0.5	0
4	0.0240	1.0	0.5	0
5	0.0013	1.0	0.5	0
6	0.0012	1.0	0.5	0
7	0.0012	1.0	0.5	0
8	0.0012	1.0	0.5	0
9	0.0085	1.0	0.5	0
10	0.0015	1.0	0.5	0
11	0.0080	1.0	0.5	0
12	0.0006	1.0	0.5	0
13	0.0004	1.0	0.5	0